



The impact of dissolved organic carbon and bacterial respiration on pCO₂ in experimental sea ice

Zhou, Jiayun; Kotovitch, Marie; Kaartokallio, Hermann; Moreau, Sebastien; Tison, Jean-Louis; Kattner, Gerhard; Dieckmann, Gerhard S.; Thomas, David N.; Delille, Bruno

Progress in Oceanography

DOI:

[10.1016/j.pocean.2015.12.005](https://doi.org/10.1016/j.pocean.2015.12.005)

Published: 01/02/2016

Peer reviewed version

[Cyswllt i'r cyhoeddiad / Link to publication](#)

Dyfyniad o'r fersiwn a gyhoeddwyd / Citation for published version (APA):

Zhou, J., Kotovitch, M., Kaartokallio, H., Moreau, S., Tison, J-L., Kattner, G., Dieckmann, G. S., Thomas, D. N., & Delille, B. (2016). The impact of dissolved organic carbon and bacterial respiration on pCO₂ in experimental sea ice. *Progress in Oceanography*, 141, 153-167. <https://doi.org/10.1016/j.pocean.2015.12.005>

Hawliau Cyffredinol / General rights

Copyright and moral rights for the publications made accessible in the public portal are retained by the authors and/or other copyright owners and it is a condition of accessing publications that users recognise and abide by the legal requirements associated with these rights.

- Users may download and print one copy of any publication from the public portal for the purpose of private study or research.
- You may not further distribute the material or use it for any profit-making activity or commercial gain
- You may freely distribute the URL identifying the publication in the public portal ?

Take down policy

If you believe that this document breaches copyright please contact us providing details, and we will remove access to the work immediately and investigate your claim.

1 **The impact of dissolved organic carbon and bacterial respiration on pCO₂**
2 **in experimental sea ice**

3

4 Zhou, J.^{1,2,3}, M. Kotovitch^{1,2}, H. Kaartokallio⁴, S. Moreau⁵, J.-L. Tison¹, G. Kattner⁶, G.
5 Dieckmann⁶, D.N. Thomas^{4,7}, B. Delille²

6

7 ¹ Laboratoire de glaciologie, DSTE, Université Libre de Bruxelles, Belgium

8 ² Unité d'océanographie chimique, MARE, Université de Liège, Belgium

9 ³ Division of Earth and Ocean Sciences, Duke University, Durham, NC, USA

10 ⁴ Marine Research Centre, Finnish Environment Institute (SYKE), Helsinki, Finland

11 ⁵ Georges Lemaître Centre for Earth and Climate Research, Earth and Life Institute, Université
12 catholique de Louvain, Louvain-la-Neuve, Belgium

13 ⁶ Alfred Wegener Institute Helmholtz Center for Polar and Marine Research, Bremerhaven,
14 Germany

15 ⁷ School of Ocean Sciences, Bangor University, Menai Bridge, United Kingdom

16

17

18 **Abstract**

19 Previous observations have shown that the partial pressure of carbon dioxide (pCO₂) in sea ice
20 brines is generally higher in Arctic sea ice compared to those from the Antarctic sea ice,
21 especially in winter and early spring. We hypothesized that these differences result from the
22 higher dissolved organic carbon (DOC) content in Arctic seawater: Higher concentrations of
23 DOC in seawater would be reflected in a greater DOC incorporation into sea ice, enhancing
24 bacterial respiration, which in turn would increase the pCO₂ in the ice. To verify this hypothesis,
25 we performed an experiment using two series of mesocosms: one was filled with seawater (SW)
26 and the other one with seawater with an addition of filtered humic-rich river water (SWR). The
27 addition of river water increased the DOC concentration of the water from a median of 142
28 μmol L⁻¹ in SW to 249 μmol L⁻¹ in SWR. Sea ice was grown in these mesocosms under the
29 same physical conditions over 19 days. Microalgae and protists were absent, and only bacterial
30 activity has been detected. We measured the DOC concentration, bacterial respiration, total
31 alkalinity and pCO₂ in sea ice and the underlying seawater, and we calculated the changes in
32 dissolved inorganic carbon (DIC) in both media. We found that bacterial respiration in ice was

33 higher in SWR: median bacterial respiration was 25 nmol C L⁻¹ h⁻¹ compared to 10 nmol C L⁻¹
34 h⁻¹ in SW. pCO₂ in ice was also higher in SWR with a median of 430 ppm compared to 356
35 ppm in SW. However, the differences in pCO₂ were larger within the ice interiors than at the
36 surfaces or the bottom layers of the ice, where exchanges at the air-ice and ice-water interfaces
37 might have reduced the differences. In addition, we used a model to simulate the differences of
38 pCO₂ and DIC based on bacterial respiration. The model simulations support the experimental
39 findings and further suggest that bacterial growth efficiency in the ice might be 0.15-0.2. It is
40 thus credible that the higher pCO₂ in Arctic sea ice brines compared with those from the
41 Antarctic sea ice were due to an elevated bacterial respiration, sustained by higher riverine DOC
42 loads. These conclusions should hold for locations and time frames when bacterial activity is
43 relatively dominant compared to algal activity, considering our experimental conditions.

44

45 **Highlights (85 characters per highlight)**

- 46 - Brine concentration/dilution causes the largest temporal changes of pCO₂ in ice
- 47 - Elevated BR due to riverine DOC addition increases pCO₂ in sea ice
- 48 - Gas exchange and the buffer effect further affect the bacterial impact on pCO₂

49

50 **Keywords (up to six)**

51 Sea ice, dissolved organic matter, carbon dioxide, bacterial activity, gas exchange

52 **1. Introduction**

53 Sea ice is formed from the freezing of seawater and covers about 6 % of the Earth's ocean
54 surface. It has a heterogeneous structure composed of a matrix of pure ice and brine inclusions.
55 Although sea ice is currently assumed to be impermeable to gas exchange in large-scale climate
56 models, theoretical considerations (Golden et al., 1998) and pioneer gas measurements (Gosink
57 et al., 1976) indicate that sea ice may be permeable under specific conditions of ice temperature
58 and salinity. Measurements of pCO₂ in sea ice and brines have been intensified in both the
59 Arctic (Crabeck et al., 2014; Geilfus et al., 2012a; Miller et al., 2011a, 2011b) and the Southern
60 Ocean (Delille, 2006; Delille et al., 2007; Geilfus et al., 2014). The motivation for these
61 measurements is to better understand the role of sea ice in the carbon cycle, including its role

62 in air-sea exchange of CO₂, and the potential feedback effects between the changing ice cover,
63 CO₂ fluxes, and climate change.

64 Current measurements indicate that sea ice may act as a source or a sink for atmospheric CO₂,
65 depending on the interplay of four processes:

66 (i) Brine concentration and dilution are associated with changes in ice temperature. When
67 cooling a sea ice sample, some of the liquid water of the brine freezes, reducing the brine
68 volume and inclusions and increasing the concentration of the impurities in the brine – this is
69 the so-called brine concentration. In contrast, when warming a sea ice sample, some of the pure
70 ice melts, increasing the volume of the brine inclusion and decreasing the concentration of the
71 impurities in brine – this is the so-called brine dilution (Hunke et al., 2011; Notz and Worster,
72 2009).

73 (ii) Biological activity, which includes the photosynthesis and respiration by organisms,
74 respectively, consumes and produces CO₂ (e.g., Papadimitriou et al., 2007).

75 (iii) The precipitation and dilution of calcium carbonate, which produces and consumes CO₂,
76 respectively (Dieckmann et al., 2010, 2008; Geilfus et al., 2013), effectively alters the CO₂
77 budget in the ice when sea ice is semi-permeable, and when the calcium carbonate precipitates
78 remain in the ice while the generated CO₂ is rejected into the under-ice water (Delille et al.,
79 2014; Rysgaard et al., 2007) or to the atmosphere (Geilfus et al., 2013; Loose et al., 2011).

80 (iv) Gas transport through sea ice is not yet well constrained, but it is commonly assumed that
81 sea ice is permeable for gas transport when its brine volume fraction is above 5 % (Golden et
82 al., 1998). Brine drainage – the intensity of which is estimated using Raleigh numbers – is
83 thought to be a significant process for ice-water exchange (Notz and Worster, 2009), while gas
84 bubble formation potentially plays an important role in air-ice exchange (Moreau et al., 2014;
85 Zhou et al., 2013). The diffusion of CO₂ through sea ice also affects air-ice exchange, but seems
86 to be much slower, i.e., less efficient than gas bubble transport (Kotovitch et al., submitted;
87 Loose et al., 2014).

88 Previous studies indicate that, for a given brine temperature, the pCO₂ in sea ice brine in the
89 Arctic Ocean (Geilfus et al., 2014, 2012a) was generally higher than that in the Southern Ocean
90 (Delille et al., 2014; Geilfus et al., 2014), especially when the average ice temperature was
91 below -4°C – which generally corresponds to the winter and early spring period (Figure 1). In
92 this study, we hypothesized that the higher pCO₂ was associated to the more intense bacterial
93 respiration in the Arctic sea ice, due to the large input of riverine particulate organic carbon

94 (POC) and dissolved organic carbon (DOC) in the Arctic Ocean (e.g., Dittmar and Kattner
95 (2003); Hansell et al. (2009)). Ice temperature is unlikely to explain the Arctic-Antarctic
96 discrepancies, because at a given temperature, the effect of brine concentration on pCO₂ is
97 expected to be the same in both hemispheres. However, the impact of DOC availability on
98 bacterial respiration and pCO₂ in sea ice has not yet been demonstrated by systematic DOC and
99 POC measurements in parallel. Therefore we performed an indoor experiment using two series
100 of mesocosms: One was filled with seawater (SW) and another with seawater and an addition
101 of filtered river water (SWR) to simulate riverine DOC input. The objective of the present paper
102 is to verify whether or not higher DOC concentrations in seawater, due to an addition of riverine
103 DOC, induce larger DOC concentrations in sea ice, which in turn enhance bacterial respiration
104 and pCO₂ in the ice.

105 **2. Material and methods**

106 **2.1 Experimental setting, and sampling routine and initial conditions**

107 The experimental setting and sampling routine has been described in Zhou et al. (2014). Briefly,
108 we ran a 19-day experiment in the Arctic Environmental Test Basin facility of the Hamburg
109 Ship Model Basin (www.hsva.de) from May to June 2012. We used 21 polyethylene
110 experimental mesocosms each with a volume of 1.2 m³. Eleven of the mesocosms were filled
111 with 1000 L of seawater from the North Sea (referred here after as SW), and the remaining ten
112 were filled with 900 L of seawater from the North Sea and 100 L of filtered river water collected
113 at a peat-dominated catchment of the River Kiiminkijoki, in Finland (referred here after as
114 SWR).

115 The addition of river water caused a significantly higher DOC concentration in the SWR
116 mesocosms (paired t-test, p<0.001): Median salinity-normalized DOC concentrations were 140
117 μmol L⁻¹ in SW and 251 μmol L⁻¹ in SWR (salinity 30.9), with a standard deviation of 3 % in
118 the SW mesocosms and 9 % in SWR. However, salinity-normalized dissolved organic nitrogen
119 (DON) was not significantly different between both mesocosm series (median of 16 μmol L⁻¹
120 in SW and 19 μmol L⁻¹ in SWR), because its concentration in river and North Sea water were
121 almost the same, and the standard deviation was relatively high (17 %) in both SW and SWR
122 mesocosms. The carbonate chemistry was also not significantly different for both mesocosm
123 series: median salinity-normalized total alkalinity was 2314 μmol kg⁻¹ in SW and 2336 μmol
124 kg⁻¹ in SWR; median salinity-normalized dissolved inorganic carbon (DIC) were 2113 μmol
125 kg⁻¹ in SW and and 2161 μmol kg⁻¹ in SWR; and median pCO₂ were 212 ppm in SW and 231

126 ppm in SWR, respectively. The salinities of the SWR mesocosms were adjusted to the SW
127 values by adding aquarium standard salt (Tropic Marin[®]). Nitrate (NO₃⁻) and phosphate (PO₄³⁻)
128) concentrations were also adjusted to concentrations that would not limit bacterial growth in
129 both series of mesocosms, and that were representative of areas in both Arctic and Southern
130 Oceans (Zhou et al., 2014).

131 Ice was grown from day 0 to 14, during which the air temperature was maintained at -14 °C,
132 and then the air temperature was increased to -1 °C to trigger a decay phase. We collected ice,
133 brine and seawater at various occasions from day 0 to day 19 for the measurements of
134 temperature, salinity, DOC, inorganic nutrients, bacterial abundance, and bacterial activity
135 (Zhou et al., 2014), as well as pCO₂ and total alkalinity.

136 Because the physical constraints were similar for both the SW and SWR mesocosms, we
137 expected bacterial activity to be the only process affecting the difference of pCO₂ in both water
138 and ice. Median bacterial abundance was 922 cells L⁻¹ in SW at the beginning of the experiment
139 and was not significantly different from the 972 cells L⁻¹ in SWR. Protists and active
140 photoautotrophs were absent in the experiment (checked by microscopy and epifluorescence
141 microscopy, respectively). As a corollary, there was no autochthonous production of DOC and
142 our experiment focuses on the impact of the additional allochthonous DOC (added by the river
143 water) on bacterial respiration and pCO₂ in both water and ice. Although photoautotrophs were
144 absent in our experiments, we believe that it would not drastically affect the verification of the
145 hypothesis, because the largest observed difference of pCO₂ in brine corresponds to the lowest
146 ice temperature (Figure 1), which mostly correspond to the ice interior (over winter and early
147 spring) where algal activity is relatively limited compared to the bacterial activity (Baer et al.,
148 2015).

149 **2.2 Brine volume fraction and Raleigh number**

150 The brine volume fraction is used here as a proxy of sea ice permeability and is calculated from
151 the ice temperature and salinity following the relationship of Cox and Weeks (1983). We
152 assume that the sea ice was permeable for a brine volume fraction exceeding 5 % (Golden et
153 al., 1998). We also calculated the Rayleigh number (Ra), which is a proxy for brine convection
154 as described by Notz and Worster (2008). Theoretically, convection is possible in an ice layer
155 (of a thickness h) when Ra exceeds 1 and decreases from the top to the bottom of that layer
156 (Notz, personal communication). We thus simply assume the critical Ra being 1 following those
157 theoretical considerations.

158 **2.3 DOC and DON**

159 Samples for the determination of dissolved organic carbon (DOC) and total dissolved nitrogen
160 (TDN) were stored frozen (-20 °C) in glass vials (Wheaton; pre-combusted at 500 °C for 5 h)
161 and determined by high temperature catalytic oxidation and subsequent non-dispersive infrared
162 spectroscopy and chemiluminescence detection, respectively (TOC-VCPN, Shimadzu). After
163 each batch of five samples, one reference standard (DOC-DSR, Hansell Research Lab,
164 University of Miami, US), one ultrapure-water blank and one potassium hydrogen phthalate
165 standard for DOC and potassium nitrate for TDN were measured. DON concentrations were
166 calculated as difference of TDN and inorganic nitrogen. The accuracy of the measurements was
167 $\pm 5\%$.

168 **2.4 Bacterial respiration**

169 Bacterial respiration has been calculated as the difference between the bacterial carbon demand
170 and bacterial production. We measured bacterial production (see below) and assumed that it
171 represented 34.8 % (bacterial growth efficiency, BGE) of the bacterial carbon demand to
172 deduce the bacterial respiration. BGE was derived as mean estimate from available sources for
173 sea-ice bacteria or bacteria in very cold temperatures (Kuparinen et al., 2011; Nguyen and
174 Maranger, 2011; Rivkin and Legendre, 2001).

175 For the bacterial production measurements, samples containing a known amount of crushed ice
176 and sterile-filtered seawater (Kaartokallio, 2004) were prepared in a cold room as follows: each
177 intact 5–10 cm ice core section was crushed using a spike and electrical ice cube crusher.
178 Approximately 10 mL of crushed ice was weighed in a scintillation vial. To better simulate the
179 brine pocket salinity and ensure an even distribution of labelled substrate, 3 ± 1 mL of sterile
180 filtered (through a 0.2 μm filter) seawater from the sample bags were added to the scintillation
181 vials. Bacterial production was measured immediately after sample collection using the [^3H]-
182 thymidine incorporation method (Fuhrman and Azam, 1982, 1980). Two aliquots and a
183 formaldehyde-fixed absorption blank were amended with [^3H]-thymidine (PerkinElmer, USA,
184 specific activity 20 Ci mmol^{-1}). The added concentration was 30 nmol L^{-1} for all sample types.
185 The samples were incubated in the dark at -0.6 °C on crushed ice in an insulated container
186 according to the projected level of activity: ice samples were incubated between 19 h and 22 h,
187 water and brine samples between 4 h and 6 h. The incubations were stopped by addition of
188 formaldehyde and samples were processed using the standard cold-TCA extraction and
189 filtration procedure. Samples were extracted for 15 minutes in ice-cold 5 % TCA and labelled
190 macromolecules collected on 0.2 μm mixed cellulose ester membrane filters (Osmonics). Filters

191 were rinsed five times with ice-cold 5% TCA and placed in clean scintillation vials. A Wallac
192 WinSpectral 1414 counter and InstaGel (Perkin-Elmer) cocktail were used in scintillation
193 counting. Bacterial production was calculated using a cell conversion factor of 2.09×10^{18} cells
194 mol^{-1} (Smith and Clement, 1990), a cell volume of $0.3 \mu\text{m}^3$ (Kaartokallio, 2004; Smith and
195 Clement, 1990) and a carbon conversion factor of $0.12 \text{ pgC } \mu\text{m}^{-3}$ (Nagata and Watanabe, 1990;
196 Pelegrí et al., 1999).

197 **2.5 pCO₂**

198 The pCO₂ of the seawater was measured *in-situ* using a custom-made equilibration system,
199 which is described in Delille et al. (2014). Briefly, the system consists of a membrane contractor
200 equilibrator (Membrana[®], Liqui-cell) that is connected to a non-dispersive infrared gas analyser
201 (IRGA, Li-Cor[®] 6262) via a closed air loop. Seawater and air flow rates through the equilibrator
202 and IRGA were approximately 2 L min^{-1} and 3 L min^{-1} , respectively. Temperature was
203 simultaneously measured *in situ* and at the outlet of the equilibrator using Li-Cor[®] temperature
204 sensors. Temperature correction of pCO₂ was applied assuming that the relation of Copin-
205 Montegut (1988) is valid at low temperature and high salinity. Data were stored on a Li-Cor[®]
206 Li-1400 data logger. All devices, except the peristaltic pump, were enclosed in an insulated box
207 that contained a 12 V power source providing enough warming to keep the inside temperature
208 above $0 \text{ }^\circ\text{C}$. Uncertainty is less than $5 \mu\text{atm}$.

209 The method for the pCO₂ measurements in ice is the same as in Geilfus et al. (2012b), but with
210 longer equilibrium times following Crabeck et al. (2014). The ice samples were cut with a band
211 saw, in a cold room at $-25 \text{ }^\circ\text{C}$ and adjusted to the container's inner volume ($4 \text{ cm} \times 4 \text{ cm} \times 4.4$
212 cm). The sample was sanded down using fine-grained sandpaper so that it fitted tightly into the
213 container to minimise the headspace volume. Then, the container was placed into a Dewar
214 vessel filled with ethanol, which was cooled to $-30 \text{ }^\circ\text{C}$ with liquid nitrogen. The container was
215 then connected to the extraction line (tap closed). The line was first evacuated down to a
216 pressure of 10^{-3} Torr, after which the container was evacuated for 5 min. The low temperature
217 of the vessel insures sea ice impermeability, i.e., the CO₂ of the ice was not vacuumed during
218 this process. The standard gas was then injected into the container at 1013 mbar. The container
219 was subsequently removed from the extraction line (tap closed), placed in a thin plastic bag and
220 submerged in a thermostatic bath (set to the *in situ* temperature, i.e., that was measured on the
221 ice samples directly after the extraction). After 20 h of equilibrium, the container was placed in
222 a Dewar filled with ethanol cooled at the *in situ* temperature and reconnected to the evacuated
223 (10^{-3} Torr) extraction line. At the same time, a water trap consisting of a Dewar filled with an

224 ethanol bath at $-65\text{ }^{\circ}\text{C}$ was placed on the line just before the GC. The gas was finally injected
225 into the GC. Immediately after the injection, the ice sample temperature was measured using a
226 calibrated thermometer (Testo 720®). Reproducibility of the measurement is 2.9%.

227 **2.6 TA and DIC**

228 Total alkalinity (TA) was measured on melted bulk ice and seawater samples. Ice cores were
229 cut at a 2 cm-depth resolution (about 50 g of ice for each section) and melted. Melted bulk ice
230 and seawater samples were poisoned with a solution of supersaturated HgCl_2 and then stored
231 in the dark, until analysis (one year after the sampling). TA was measured by open-cell titration
232 with 0.11 M HCl and the endpoints were determined according to Gran (1952). Routine
233 analyses of Certified Reference Materials (provided by A. G. Dickson, Scripps Institution of
234 Oceanography) ensured that the uncertainty of the TA measurements was less than $4\text{ }\mu\text{mol kg}^{-1}$.

235 Dissolved inorganic carbon (DIC) was calculated from TA and pCO_2 using CO2SYS (Lewis
236 and Wallace, 1998), the CO_2 acidity constants of Mehrbach et al. (1973) refitted according to
237 Dickson and Millero (1987) and other constants advocated by DOE (1994). We assumed that
238 the CO_2 dissociation constants were applicable at sub-zero temperatures as suggested by
239 Marion (2001) and Delille et al. (2007). To compare DIC in seawater and in melted bulk ice,
240 we normalized the DIC values to a salinity of 7 (DIC_7), for consistency with previous studies.
241 The salinity of 7 is also the mean salinity of the ice in this study. Uncertainty of DIC_7 deduced
242 from the reproducibility of TA and pCO_2 has been evaluated to be $0.8\text{ }\mu\text{mol kg}^{-1}$ using Monte
243 Carlo procedure (Anderson, 1976).

244 **2.7 Differences between the SW and SWR series and statistical tests**

245 The ice thickness was different between the SW and SWR mesocosms (up to 3 cm (15 %) of
246 difference) at day 14 and day 15. This was due to an unavoidable temperature gradient in the
247 experimental basin (Zhou et al., 2014). In spite of the gradient of temperature in the
248 experimental basin, we do not think that it has affected the results. The SW and SWR
249 mesocosms sampled the same day were adjacent mesocosms located on the same row
250 (minimizing the differences in physical conditions). For day-to-day sampling, the SW/SWR
251 pairs of mesocosms were randomly selected in space. In spite of that random selection, we still
252 could see a trend in the physical parameters (Zhou et al., 2014), which means that the
253 temperature gradient in the experimental basin did not significantly bias our results. However,
254 to be rigorous, when the ice thicknesses were different for SW and SWR, we calculated the
255 difference of the parameters (e.g., pCO_2) on normalized ice depth, and then multiplied the

256 normalized ice depth by the ice thickness of the SW series. In addition, two parameters were
257 assumed to be similar (i.e., no significant difference between the SW and SWR series), when a
258 minimum similarity score of 0.95 was achieved.

259 **3. Results**

260 **3.1 Physical sea ice conditions**

261 As described in Zhou et al. (2014), the differences in the physical properties of the ice between
262 the SW and SWR mesocosms were insignificant. The brine volume fraction was above 5 %
263 during the whole experiment, which suggests that the ice was always permeable (Golden et al.,
264 1998). The maxima in the brine volume fraction were all found at the bottom of the ice, while
265 the minima were found in the ice interior, and decreased from 13.3 % on day 1 to 5.7 % on day
266 14, but increased from day 15 onwards, due to the increase of the air temperature from -14 °C
267 to -1 °C. The Rayleigh numbers were higher than 1, indicating favourable conditions for brine
268 convection at all ice depths on day 2, and thereafter only at the bottom of the ice until day 14.
269 From day 15 onwards, the Rayleigh numbers were always below 1, indicating that brine
270 convection was unlikely (Figure 2). A large difference of Ra has been observed at the bottom
271 of the ice between SW and SWR mesocosms, from day 6 to 14, and was likely due to an
272 underestimation of salinity in SWR, and the propagation of that bias in the calculation of Ra
273 (Zhou et al., 2014), but is not significant for the purpose of the present study.

274 **3.2 DOC and DON**

275 DOC concentrations in sea ice and water and their difference between the SW and the SWR
276 mesocosms have been presented and discussed in Zhou et al. (2014) and Jørgensen et al. (2015).
277 Most importantly, the salinity-normalized DOC concentrations in the underlying water were
278 higher in the SWR mesocosms than in the SW mesocosm during the experiment (paired t-test,
279 $p < 0.001$); the medians were $142 \mu\text{mol L}^{-1}$ in SW and $246 \mu\text{mol L}^{-1}$ in SWR (salinity of 30.9),
280 which were similar to the initial conditions. Median DOC concentrations in ice were $71 \mu\text{mol}$
281 L^{-1} in SW and $109 \mu\text{mol L}^{-1}$ in SWR. These are equivalent to $287 \mu\text{mol L}^{-1}$ and $409 \mu\text{mol L}^{-1}$
282 respectively, once normalized to a salinity of 30.9 as for the underlying water (paired t-test,
283 $p < 0.001$); they are higher than the values in water, which indicate a preferential retention of
284 DOC in sea ice.

285 DON concentrations have not been systematically measured as for DOC ($n=18$ in water and 15
286 in ice for DON compared to $n=20$ and 110, respectively, for DOC (SW+SWR)). The limited

287 number of data we have show that the salinity-normalized DON concentrations were not
288 significantly different in SW and SWR mesocosms, not before the experiment (median of 21
289 $\mu\text{mol L}^{-1}$), or during the experiment, in both the water and ice (medians of 17 $\mu\text{mol L}^{-1}$ and 21
290 $\mu\text{mol L}^{-1}$, respectively) (data not shown). No significant trend in DON has been detected in the
291 water and the ice over the experiment.

292 **3.3 Bacterial activity**

293 Median bacterial abundance in the underlying water increased over the experiment, reaching
294 1470 cells L^{-1} in SW and 1505 cells L^{-1} in SWR. This difference was not significant, despite
295 the significantly higher bacterial production (BP) in the SWR mesocosms (paired t-test,
296 $p=0.007$), with a median of 69 $\text{nmolC L}^{-1} \text{h}^{-1}$ in SWR compared to 51 $\text{nmolC L}^{-1} \text{h}^{-1}$ in SW.
297 Bacterial respiration (BR) in water was also higher in the SWR mesocosms (paired t-test,
298 $p=0.027$), with a median of 98 $\text{nmolC L}^{-1} \text{h}^{-1}$ in SW and 129 $\text{nmolC L}^{-1} \text{h}^{-1}$ in SWR, respectively
299 (Figure 3a, left).

300 Median bacteria abundance in ice was 299 cells L^{-1} in SW and 352 cells L^{-1} in SWR, with a net
301 loss of 24 cells $\text{L}^{-1}\text{d}^{-1}$ in SW and 16 cells $\text{L}^{-1}\text{d}^{-1}$ in SWR over the experiment. Median BP was 5
302 $\text{nmolC L}^{-1} \text{h}^{-1}$ in SW and 13 $\text{nmolC L}^{-1} \text{h}^{-1}$ in SWR, and median BR, 10 $\text{nmol L}^{-1} \text{h}^{-1}$ in SW and
303 25 $\text{nmol L}^{-1} \text{h}^{-1}$ in SWR (Fig. 3a, right). To compare bacterial activity in ice with that in
304 seawater, we assumed that all these parameters were conservative against salinity. Once
305 normalized to a salinity of 30.9, median bacterial abundance reached 1220 cells L^{-1} in SW and
306 1440 cells L^{-1} in SWR; median BP of 23 $\text{nmolC L}^{-1} \text{h}^{-1}$ in SW and 53 $\text{nmolC L}^{-1} \text{h}^{-1}$ in SWR;
307 and median BR of 42 $\text{nmolC L}^{-1} \text{h}^{-1}$ in SW and 100 $\text{nmolC L}^{-1} \text{h}^{-1}$ in SWR. Note that all these
308 values were higher in SWR than in SW (paired t-test, $p<0.001$), but lower than in seawater
309 (paired t-test, $p<0.001$ for BP and BR in SWR; $p=0.001$ in SW; $p=0.004$ for bacterial abundance
310 in SW but no significance has been found for bacterial abundance in SWR). The vertical
311 distribution of BR in ice was similar in the SW and SWR mesocosms (Figure 4): It increased
312 from the top to the bottom of the ice. The difference between both mesocosm series generally
313 increased from the top to the bottom of the ice, where the largest differences were observed.

314 **3.4 DIC₇**

315 For data comparison with literature, we normalized DIC to a salinity of 7. Differences of DIC₇
316 between SW and SWR were not significant for both the under-ice water and the ice. DIC₇ in
317 seawater varied around a median value of 455 $\mu\text{mol kg}^{-1}$, when excluding the outlier of SWR
318 on day 5. Median DIC₇ in ice for the same mesocosms was slightly higher than in seawater,

319 reaching $486 \mu\text{mol kg}^{-1}$ (Figure 3). DIC_7 in both media increased from day 2 to day 16 and then
320 remained constant. DIC_7 in the ice increased from the top to the bottom of the ice in SW and
321 SWR mesocosms (Figure 5). At the bottom of the ice, it increased throughout the experiment
322 and was always higher than the DIC_7 of the under-ice water by an average of $40 \mu\text{mol kg}^{-1}$. The
323 difference of DIC_7 between SWR and SW was higher in the ice interior at 8 cm to 12 cm depth.
324 For comparison with bacterial respiration in ice, median DIC in ice that is not salinity-
325 normalized was $434 \mu\text{mol kg}^{-1}$, which is equivalent to $400 \mu\text{mol L}^{-1}$.

326 **3.5 pCO₂**

327 pCO₂ in water was not significantly different between both mesocosm series, with a median
328 pCO₂ of 270 ppm. pCO₂ in ice was also not significantly different between both mesocosm
329 series probably as a result of the large variability. Median pCO₂ in ice was 360 ppm with a large
330 range spanning from 223 ppm to 651 ppm (Figure 3). Median pCO₂ was higher in the ice than
331 in seawater during ice growth (day 2 to day 14), despite similar concentrations of DIC_7 in the
332 seawater and in the ice and lower bacterial respiration in ice than in seawater (Figure 3c,
333 sections 3.3 and 3.4).

334 The pCO₂ in ice had a similar temporal evolution in the SW and SWR mesocosms (Figures 3c
335 and 6). Considering that the average atmospheric pCO₂ was 460 ppm during the experiment
336 (Kotovitch et al. submitted), pCO₂ in ice was at first under-saturated on day 2, and then became
337 increasingly supersaturated until day 14, and then under-saturated again from day 15 onwards.
338 Despite the similar temporal evolution of pCO₂ in ice, pCO₂ was generally higher in the SWR
339 mesocosms, with a median value of 430 ppm compared to the 356 ppm in the SW mesocosms.
340 The differences in pCO₂ were generally higher from the top to the ice interior to about 8 cm
341 depth, except on day 2, when the ice was relatively thin (6 cm); on days 5 and 19, the difference
342 of pCO₂ at the bottom of the ice was likely biased due to the large difference of CO₂ in the
343 under-ice water (Figure 3c, left). Indeed, for days 5 and 19, the differences in pCO₂ in the under-
344 ice water between SW and SWR were 100 ppm and 86 ppm, respectively, while they generally
345 approached 0 ppm to 20 ppm in the other mesocosms on all other sampling days (Figure 3c,
346 left).

347 **4. Discussion**

348 The addition of river water led to an enrichment of the overall DOC concentrations in the SWR
349 water, compared to SW, by a factor of 1.8 ($251 \mu\text{mol L}^{-1} / 140 \mu\text{mol L}^{-1}$). The preferential
350 retention of DOC in sea ice during ice formation (Giannelli et al., 2001; Müller et al., 2013;

351 Zhou et al., 2014) led to a salinity-normalized DOC concentration in ice that was higher than
352 the under-ice water ($409 \mu\text{mol L}^{-1} / 287 \mu\text{mol L}^{-1}$), but the difference of DOC enrichment
353 between SWR and SW dropped to 1.4. The mechanisms underlying the preferential retention
354 of DOC in sea ice is not fully understood, but other measurements during our experiment
355 suggested that sea ice formation increases the lability of DOM in ice (Jørgensen et al., 2015).
356 We therefore speculate that the more labile forms of DOM were better retained in sea ice than
357 the more refractory ones. Because SWR contained a larger fraction of less labile terrestrial
358 humic acids due to the addition of river water (Jørgensen et al., 2015), the DOC enrichment in
359 ice in SWR was lower than in SW. We show below that the segregation of DOC between water
360 and ice, in addition to the difference in temperature and salinity, likely contributed to the
361 difference of bacterial activity in water and ice.

362 **4.1 Impact of riverine DOC addition on bacterial activity**

363 Available under-ice or partially ice covered water respiration estimates for Western Arctic vary
364 from 19 to 39 $\text{nmol C L}^{-1} \text{h}^{-1}$ (Kirchman et al., 2009; Nguyen and Maranger, 2011; Nguyen et
365 al., 2012), which is an order of magnitude lower than our respiration estimate for water (median
366 of 98 $\text{nmol C L}^{-1} \text{h}^{-1}$ in SW and 129 $\text{nmol C L}^{-1} \text{h}^{-1}$). However, our experimental system was
367 based on North Sea water with a high DOC content and added inorganic nutrients, which are
368 both likely to support higher bacterial production than the more oligotrophic Arctic waters.

369 Assuming that bacterial activity took place 24 hours a day, a consumption of 23.3 $\mu\text{mol C L}^{-1}$
370 in SW and 31.5 $\mu\text{mol C L}^{-1}$ in SWR is necessary to support the observed BP over the 19-day
371 experiment. These represent 16 % and 13 % of the DOC pool, respectively. However, no
372 significant changes have been detected in the DOC and DON concentrations in the under-ice
373 water, or in the concentrations of inorganic nutrients (Zhou et al., 2014). A possible explanation
374 is that bacteria used particulate organic matter (POM) as a carbon source for growth, despite
375 the large pool of DOC. We did not measure POM concentrations in our experiment, but
376 considering the absence of protists and active algae in seawater (in spite of the use of unfiltered
377 seawater), we assumed that they died in the mesocosms, providing an additional source of
378 carbon for bacterial growth. If this assumption is correct, BP would represent a smaller fraction
379 of the DOC pool. The fraction was likely smaller than 3 % in SW and 9 % in SWR (the standard
380 deviation of DOC concentrations among the mesocosms in the initial waters), because we
381 would have detected significant changes otherwise.

382 Although BP only represented a small fraction of the DOC pool, the addition of riverine DOC
383 was the most plausible factor causing the significantly higher BP in the SW water, since all the
384 other parameters (bacterial abundance, DON, inorganic nutrients, temperature, and presumably
385 POC) were not significantly different between the SW and SWR mesocosms.

386 Published sea-ice respiration values originate from batch culture incubations using sea ice
387 bacteria and are either derived from total Arctic sea ice community respiration measurements
388 made in water phase incubations (Nguyen and Maranger, 2011) or from experimental systems
389 with Baltic sea ice bacteria (Kuparinen et al., 2011). The estimated mean bacterial respiration
390 in western Arctic ice was $50 \text{ nmol C L}^{-1} \text{ h}^{-1}$ (Nguyen and Maranger, 2011) and in the Baltic Sea
391 experiments approximately $80 \text{ nmol C L}^{-1} \text{ h}^{-1}$ (Kuparinen et al., 2011). Our respiration estimate
392 for ice was lower but of the same order of magnitude, despite major differences in methodology
393 and experimental setup.

394 Bacterial activity in ice was different from that in the under-ice water. Bacterial abundance in
395 sea ice was lower than in seawater, even when normalized to the same salinity. This has been
396 observed before in similar experiments (Eronen-Rasimus et al., 2014) and likely resulted from
397 the low ice temperature and high brine salinity, which favour the selection of psychrotrophic
398 and psychrophilic bacteria (Helmke and Weyland, 1995).

399 Although the overall BP and bacterial abundance were lower in the ice than in the under-ice
400 water, the ratio between both the SW and SWR mesocosms were more pronounced in the ice.
401 Bacterial production in SWR ice was 2.6 times higher than in SW, i.e., twice as high as the ratio
402 (SWR/SW) observed in the water. Bacterial abundance was 20 % higher than the SW ice, while
403 no significant difference was found in the under-ice water. The only plausible factor driving
404 these SWR/SW differences in ice was the higher DOC concentration in the SWR ice. Ice
405 microalgae and protists were indeed absent (verified by microscopy) and no significant
406 difference has been found in the DON concentrations and the physical properties of the ice.

407 It is curious as to why the differences of BP between both series of mesocosms were larger in
408 ice (SWR/SW ratio of 2.6) than in the water (ratio of 1.3), considering that the differences of
409 DOC concentrations between both mesocosms series decreased (ratio of 1.4 in ice compared to
410 1.8 in water). This might be associated with the changes of the organic matter quality towards
411 more labile (bioavailable) forms in the ice during sea ice formation (Jørgensen et al., 2015). In
412 seawater, the addition of riverine DOC promoted higher BP in the SWR mesocosms. In sea ice,
413 the absolute DOC concentrations in SWR are not only higher than in SW, their lability might
414 also have increased compared to the SWR under-ice water; both might explain the larger

415 difference of BP in ice between the SW and SWR mesocosms compared to the under-ice water.
416 DOC can directly contribute to bacterial growth as a carbon source; it may also support the
417 formation of exopolymeric substances (EPS) in growing sea ice (Aslam et al., 2012) – a
418 substance that is known to support microorganisms survival under the extreme conditions in
419 sea ice (Krembs et al., 2011). Further, it might also have favoured the development of a bacterial
420 community that is different from that in SW, as it has been observed by Eronen-Rasimus et al.
421 (2014).

422 **4.2 Similarities of DIC and pCO₂ in ice in the SW and SWR mesocosms**

423 DIC₇, which ranged from 423 μmol kg⁻¹ to 512 μmol kg⁻¹ (in SW and SWR), was consistent
424 with previous measurements on natural sea ice (Geilfus et al., 2014, 2012a; Rysgaard et al.,
425 2007). pCO₂ measurements for natural sea ice are scarce (Crabeck et al., 2014; Geilfus et al.,
426 2014) and have been mainly obtained from the spring-summer period. Therefore, they were
427 generally under-saturated relative to the atmosphere (i.e., below 400 ppm) (Crabeck et al., 2014;
428 Geilfus et al., 2014). The pCO₂ below 400 ppm in ice during the decay period of our experiment
429 was thus consistent with data from natural sea ice in spring and summer. Because of the lack
430 of pCO₂ measurements in natural ice during ice growth (and especially in autumn), we extended
431 the comparison to the pCO₂ in brine. Considering that the median ice temperature approached
432 -4.5 °C during ice growth in this experiment (Zhou et al., 2014), and that temperature would
433 correspond to a pCO₂ of about 800 ppm in Arctic sea ice brine (Figure 1), our in situ
434 measurements of up to 724 ppm are realistic.

435 Brine concentration and dilution and gas transport are likely to be the two main physical
436 processes determining the similarities in the temporal and vertical pattern of pCO₂ between the
437 SW and SWR mesocosms (Figure 7). When plotting pCO₂ in ice (SW and SWR) against the
438 brine volume fraction, 10 mesocosms over 14 (represented by the circles on Figure 7) followed
439 a decreasing trend ($r^2 = 0.836$, $p < 0.03$). These events include the very beginning of ice growth
440 (day 2) and the ice growth and ice decay, except day 5, day 15 and two other outliers.

441 When cooling an ice sample, part of the water present in the brine inclusion will freeze, forming
442 a thicker surrounding pure ice matrix, which results in a higher concentration of the dissolved
443 constituents into smaller brine inclusions. Therefore, pCO₂ in sea ice became increasingly
444 supersaturated, as the brine volume fraction decreased (from day 0 to day 14). In contrast, when
445 warming an ice sample, the surrounding pure ice matrix is expected to melt, increasing the size
446 of the brine inclusion and diluting the concentration of the dissolved constituents in the brines.

447 pCO₂ in sea ice thus became under-saturated as a result of the warming air temperature (from
448 day 15 onwards) (Figures 6 and 7).

449 A rapid and one-time decrease of pCO₂ in ice was observed on day 15. This was a particular
450 event, occurring the day after the rapid increase of the air temperature, when the sea ice surface
451 temperature sharply increased from -10 °C to -2 °C within 20 hours (Kotovitch et al.,
452 submitted). Different processes may explain this drastic decrease of pCO₂, e.g., rapid release
453 of gas bubbles (Zhou et al., 2013) and/or melt of CO₂-poor surface ice layers and seepage of
454 the meltwater (Geilfus et al., 2014), while the equilibrium of air-ice pCO₂ occurs at a much
455 slower rate. However, considering that day 15 was a particular event, it is unlikely that these
456 pCO₂ changes would be representative of those observed in natural conditions, so we will not
457 further discuss the different plausible processes. Another outlier corresponded to the surface
458 ice layer, where ice melt might have induced the low pCO₂ (153 ppm). We currently have no
459 explanation for the other outlier on day 5. Nevertheless, excluding these data, pCO₂ was
460 significantly correlated with the brine volume fraction, which indicates the major role of brine
461 concentration and dilution in regulating pCO₂ in ice.

462 To further demonstrate the importance of brine concentration and dilution for pCO₂ dynamics,
463 we compared our values with the theoretical pCO₂ considering only the changes in temperature
464 and brine salinity. The theoretical pCO₂ was calculated using the CO2SYS program (Lewis and
465 Wallace, 1998), the constants of Goyet and Poisson (1989), and the median temperature,
466 salinity, total alkalinity and DIC in the parent water as initial conditions. We then used the
467 median ice salinity (6.3) to calculate the brine volume fraction associated with each prescribed
468 temperature. The theoretical pCO₂ (red curve in Figure 7) reproduced the observations well
469 between 10 % and 20 % of brine volume fraction (i.e., for about half of the data set), but
470 overestimated the pCO₂ in ice (up to 320 ppm, i.e., 44 %) for brine volume fractions below 10
471 %. We attribute this overestimation to a significant escape of CO₂ from the ice to the
472 atmosphere during ice growth, which is not taken into account by the CO2SYS. Another
473 explanation could be that the constants used in CO2SYS might be incorrect for sea ice, since
474 they were developed for temperature and salinity ranges of seawater, which are less extreme
475 than those of sea ice. However, the error in the estimate of pCO₂ should approach 10 %
476 according to Brown et al. (2014), when using TA and DIC as input parameters and the constants
477 of Goyet and Poisson (1989). Hence, the error on the seawater-derived constant is not great
478 enough to explain the difference in pCO₂ between the CO2SYS estimate and the observations,

479 and therefore the escape of CO₂ from the ice to the atmosphere remains the most plausible
480 explanation.

481 The DIC₇ profiles confirm that gas transport through sea ice affected pCO₂ in ice (Figure 5), in
482 addition to brine concentration and dilution. If sea ice would be a closed system, and the air-ice
483 and ice-water exchange absent, DIC would be conservative against salinity. Hence, the value
484 of DIC₇ would be the same at all ice depths and in seawater. In our study, the ice was always
485 permeable, with the brine volume fraction always above 5 % (Golden et al., 1998). Gas
486 exchange through the ice was thus possible and resulted in the deviation of the DIC₇ in ice from
487 the conservative behaviour. Values of DIC₇ in ice that decreased from the bottom to the top of
488 the ice indicate an escape of CO₂ from the surface of the ice to the atmosphere (Figure 5)
489 (Geilfus et al., 2013), and the observed decrease was also consistent with the air-ice fluxes we
490 have measured during the growth phase of this experiment (Kotovitch et al., submitted). At the
491 bottom of the ice, DIC₇, which approached the values in the under-ice water, indicate that ice-
492 water exchange took place, which was possible through brine convection (high Rayleigh
493 number, Figure 2). The DIC₇ at the bottom of the ice increased throughout the entire period of
494 ice growth, following the increase in DIC₇ in the under-ice water as a result of the expulsion of
495 DIC from the ice and bacterial respiration in the water during ice growth (Figure 3) (Moreau et
496 al., submitted).

497 **4.3 Differences of DIC and pCO₂ in ice between the SW and SWR mesocosms**

498 DIC₇ and pCO₂ in ice were higher in SWR than in SW. However, these differences between
499 SW and SWR were not significant, despite the significantly higher BR in SWR, which should
500 result in a larger accumulation of DIC and CO₂ in SWR. Because the dynamics of DIC₇ and
501 pCO₂ not only depend on bacterial activity, but also on physical processes (which were the same
502 in both SW and SWR), the absence of significant differences might indicate that the physical
503 processes have offset the bacterial impact on DIC₇ and pCO₂. For instance, if the differences of
504 DIC₇ and pCO₂ were only due to bacterial activity, it is curious as to why the largest differences
505 of DIC₇ and pCO₂ were observed in the ice interior (Figures 5 and 6), instead of at the bottom
506 of the ice, where the difference in bacterial respiration was the largest. We interpret this as the
507 result of gas exchange at the air-ice and ice-water interfaces, in addition to bacterial respiration.
508 Since the difference of pCO₂ was smaller between the bottom of the ice and the water than
509 between the surface of the ice and the atmosphere, we conclude that ice-water exchange might
510 have been more efficient than air-ice exchange in decreasing the difference of pCO₂ between
511 SWR and SW due to bacterial respiration. This is in agreement with the higher Rayleigh

512 numbers observed at all times at the bottom of the growing sea ice, that indicate enhanced
513 convection and therefore exchanges with the under-ice water.

514 Bacterial respiration in bulk ice ($10 \text{ nmolC L}^{-1} \text{ h}^{-1}$ in SW and $25 \text{ nmolC L}^{-1} \text{ h}^{-1}$) over 19 days
515 only represent 1 to 3% of the stock of DIC ($400 \text{ } \mu\text{molC L}^{-1}$). It is therefore curious as to how
516 such a low bacterial respiration may have caused a significant difference of pCO_2 in the ice
517 interior. An explanation could be the increase of the buffering effect of the carbonate system
518 with the decrease of temperature and the increase of salinity in brine (brine concentration). The
519 chemical buffer factor ($\beta = \Delta\text{pCO}_2/\Delta\text{DIC}$) describes the change in pCO_2 relative to the DIC
520 change induced by an input (i.e., respiration) or output of dissolved CO_2 . It results from the
521 interplay of equilibrium dissociation reactions of the carbonate system and is a function of
522 several physico-chemical conditions (Delille et al., 2005; Frankignoulle, 1994). In a closed
523 system, β of brines increases significantly with decreasing temperature and the associated
524 increase of brine salinity (Figure 8). Providing that bacterial respiration could explain the
525 accumulation of DIC, an increase of DIC (even small) can result in a larger increase in pCO_2
526 in cold saline brine compared to warmer underlying seawater (Figure 8). Considering that the
527 difference of DIC_7 in the ice interior approached $15 \text{ } \mu\text{mol kg}^{-1}$ (Figure 5) and that at β
528 approached 4 at $-4.5 \text{ }^\circ\text{C}$ (median temperature of the ice), an expected difference of pCO_2 due
529 to buffer factor changes should approach 60 ppm, which is relatively close to our observation
530 (Figure 6).

531 An alternate explanation is the underestimation of the bacterial respiration in bulk ice. We
532 calculated bacterial respiration based on thymidine incorporation and different conversion
533 factors. Our choice of BGE might have led to an underestimation of the estimate of bacterial
534 respiration, as discussed in the next section,.

535 **4.4 Modelling the impact of bacterial respiration on pCO_2 in ice**

536 In a closed system, bacterial respiration would induce an accumulation of DIC. In our semi-
537 enclosed system, DIC also changed due to physical processes (ice-air and ice-water exchanges).
538 The interplay of these various processes makes it difficult to use a simple calculation to prove
539 (i) whether the difference in bacterial respiration caused the observed difference of DIC and
540 pCO_2 in the ice interior, and (ii) whether ice-air and ice-water exchanges have offset the
541 difference of DIC and pCO_2 caused by respiration at the surface and the bottom of the ice,
542 respectively.

543 To tackle these issues, we used the one-dimensional thermodynamic sea ice model of Moreau
544 et al. (2015) which includes ice-air gas exchanges and sea ice carbon dynamics. The model
545 features ice growth and melt, ice-air and ice-water exchanges, as well as representations of full
546 inorganic carbon and basic organic carbon dynamics within the ice. For the model simulations,
547 all the parameters used are those described in Moreau et al. (2015), except for biological activity
548 where primary production was shut down in the model runs. Bacterial respiration is prescribed
549 with the median values of the bacterial respiration for SW and SWR, i.e., $10 \text{ nmol C L}^{-1} \text{ h}^{-1}$ in
550 SW and $25 \text{ nmol C L}^{-1} \text{ h}^{-1}$ in SWR, which corresponded to the use of a bacterial growth
551 efficiency (BGE) of 0.348. Based on the initial conditions of the experiment, we prescribed the
552 initial seawater TA and DIC concentrations ($2244 \text{ } \mu\text{mol kg}^{-1}$ and $2039 \text{ } \mu\text{mol kg}^{-1}$, respectively)
553 and the initial sea ice TA and DIC concentrations ($847 \text{ } \mu\text{mol kg}^{-1}$ and $748 \text{ } \mu\text{mol kg}^{-1}$). The
554 model was run over 19 days (duration of the experiment), with a 1-hour time step.

555 Because the model has different temporal and spatial resolutions than the observations, we
556 decided to only compare the temporal evolution of the median values in the ice (modelled
557 versus measured variables). Overall, the model reproduced the ice thicknesses, median ice
558 temperatures and salinities, as well as the standing stock of DIC and the median pCO_2 in ice in
559 the same magnitude as those observed (Figure 9).

560 We first ran the model with the median values of the observed bacterial respiration for SW and
561 SWR by using a BGE of 0.348 (Kuparinen et al., 2011). Given these bacterial respiration rates,
562 the model reproduces the spatial pattern of the observed DIC_7 standing stock and the median
563 pCO_2 (Figure 9) but not the magnitude of their difference between SW and SWR (Table 1).
564 Therefore, we re-calculated bacterial respiration rates for SW and SWR using different BGE.
565 Reducing BGE to 0.2 or 0.15 is plausible considering that BGE ranges from 0.05 to 0.6 (i.e.,
566 from 5 % to 60 %), depending on the environmental conditions (e.g., the quality of the dissolved
567 organic matter) (Del Giorgio and Cole, 1998; Nguyen et al., 2012; Rivkin and Legendre, 2001).

568 Firstly, changing the BGE to 0.2 or 0.15, and hence increasing the BR, did not change the total
569 stock of DIC and the median pCO_2 significantly (Figure 9, coloured curves), which supports
570 our previous suggestions about the importance of the physical processes, such as brine
571 concentration and dilution and gas transport, in regulating the dynamics of DIC and pCO_2 in
572 sea ice. However, changing the BGE to 0.2 or 0.15 enhanced the differences in DIC_7 and pCO_2
573 in ice between SW and SWR (Table 1). The modelled median difference of DIC_7 fits the
574 observations better when using a BGE of 0.2 and 0.15 (Table 1), and considering the
575 reproducibility of $\pm 0.8 \text{ } \mu\text{mol kg}^{-1}$ for DIC. The median difference of pCO_2 is then higher than

576 the observed differences in $p\text{CO}_2$ between SW and SWR, but considering that the model slightly
577 overestimates the $p\text{CO}_2$ near the ice surface (*Kotovitch et al.*, submitted), differences in DIC_7 ,
578 rather than $p\text{CO}_2$, would be a better indicator of the difference in bacterial impact. The model
579 simulations therefore suggest that the bacterial respiration in ice might be up to 3 times higher
580 than our previous estimate (Table 1).

581 The estimate of BGE for the entire period of the experiment (0.15 - 0.2), as suggested by the
582 model simulations, was lower than assumed. Our BGE estimate of 0.348 was based on
583 empirical values obtained in liquid batch cultures in above-zero temperature (Kuparinen et al.
584 2011, Nguyen and Maranger 2011) combined with calculated temperature-dependent estimate
585 (Rivkin & Legendre 2001). Measuring bacterial process rates, especially respiration in sea-ice
586 systems is complicated and direct respiration measurements were not available. The lower
587 actual BGE suggested by the model in our experimental system compared to the previous
588 published values is plausible because of the extremely low temperatures and high salinities in
589 brine. Extreme conditions are in general forcing bacteria to invest more energy for survival than
590 for growth. Along these lines, the actual BGE may vary throughout the ice growth, being lower
591 during ice growth (where the conditions were more extreme), and higher during ice melt (where
592 the conditions were milder). Further investigations are encouraged to verify this hypothesis.
593 Furthermore, BGE in water column and ice may be different with higher BGE in water where
594 conditions are less extreme. Higher BGE from 0.4 to 0.5 were suggested by Moreau et al.
595 (submitted) for the under-ice water, in the same experimental system. Higher BGE for under-
596 ice water would also lower the respiration estimate towards values measured in other studies
597 (Kirchman et al. 2009, Nguyen and Maranger 2011, Nguyen et al. 2012) albeit in the high Arctic
598 under different nutrient and dissolved organic carbon regimes.

599 The comparison of Figure 5 with Figure 10, and Figure 6 with Figure 11 shows that the model
600 reproduced the temporal and spatial pattern of DIC_7 and $p\text{CO}_2$ well. DIC_7 decreased from the
601 bottom to the top of the ice due to air-ice gas exchange, except in the bottom most layer where
602 DIC_7 is underestimated due to an improper parameterization of heat and salt transfer in this
603 layer (Moreau et al., 2014; Vancoppenolle et al., 2010). $p\text{CO}_2$ was supersaturated in the ice
604 during the entire ice growth period, except in the bottom layer where brine convection pulled
605 the $p\text{CO}_2$ towards the under-saturated $p\text{CO}_2$ value of the under-ice water. $p\text{CO}_2$ in ice then also
606 became under-saturated, as it was observed, as a result of the increase of air temperature (and
607 the related brine dilution). In addition, due to the higher bacterial respiration in SWR compared
608 to SW, DIC_7 and $p\text{CO}_2$ were higher in SWR than in SW. The differences of $p\text{CO}_2$ are alleviated

609 at the bottom of the ice because of brine convection, and slightly at the top of the ice due to air-
610 ice gas exchange, but they are greater in the ice interior, which has to be associated with the
611 difference in bacterial respiration – the sole difference between the two runs: SW and SWR.

612 There are two main differences between the model simulations and the observations: The
613 absolute values of DIC₇ and pCO₂ are higher in the model than in the observations, and the
614 differences of DIC₇ and pCO₂ between SWR and SW present a smoother pattern in the model
615 than in the observations (Figures 5, 6, 9 and 10). Ice-air gas fluxes are currently not yet well
616 constrained in the model, resulting in a slight underestimation of the ice-air gas fluxes, and thus
617 an overestimation of the modeled DIC and pCO₂ content in the ice (Kotovitch et al., submitted).
618 The smoother pattern in the modelled differences of DIC₇ and pCO₂ may result from the higher
619 spatial and temporal resolution in the model than in the observations: Hourly time step and
620 calculation on the 10 ice layers in the model compared to the almost daily sampling with 1 to 4
621 measured ice layers on each ice core.

622 In brief, differences exist between the model simulations and the observations, probably due to
623 the parameterization of air-ice gas exchange and the difference of spatial and temporal
624 resolution, but the model was able to reproduce the temporal and spatial patterns of DIC₇ and
625 pCO₂, confirming therefore the importance of brine concentration and dilution, and gas
626 transport in controlling their dynamics. Most importantly, the model reproduced the observed
627 median difference of DIC₇ in the ice by introducing the measured bacterial respiration (for a
628 lower BGE of 0.15 or 0.2), confirming that higher bacterial respiration could indeed cause a
629 larger accumulation of DIC and a larger pCO₂ in the ice.

630 A corollary to the higher bacterial respiration, DIC and pCO₂ in SWR in the model is an
631 enhanced ice-air CO₂ flux during ice growth by 17 % (1.68 mmol m⁻² d⁻¹ and 1.97 mmol m⁻² d⁻¹
632 ¹ in SW and SWR, respectively), and a reduced CO₂ flux during ice decay by 38 % (-1.52 mmol
633 m⁻² d⁻¹ and -0.93 mmol m⁻² d⁻¹ in SW and SWR, respectively) if we assume a BGE of 0.15
634 (simulated fluxes not shown). The enhanced CO₂ fluxes during ice growth are obviously due to
635 the higher pCO₂ in the ice resulting from the higher bacterial respiration. The negative CO₂
636 fluxes (i.e., from the air to the ice) are due to brine dilution (e.g., Nomura et al., 2010), and the
637 flux is less negative in SWR because the larger bacterial respiration in SWR better compensates
638 the effect of brine dilution. The integrated CO₂ flux over the 19 days of the simulation was 0.16
639 mmol m⁻² d⁻¹ and 1.04 mmol m⁻² d⁻¹ in SW and SWR, respectively. Hence, the addition of DOC
640 might have induced an air-ice CO₂ flux that was more than 6 times higher than without the
641 addition of DOC.

5. Conclusion and large scale implications

642 The aim of the study was to verify the hypothesis as to whether a larger input of riverine DOC
643 in the Arctic water could induce a higher DOC concentration in sea ice, which would promote
644 bacterial respiration, leading to a higher $p\text{CO}_2$ in brine. Although the overall trend of $p\text{CO}_2$ in
645 both mesocosm series strongly depends on the ice temperature (Figure 1) as a result of the effect
646 of brine concentration and brine dilution, the differences (SWR-SW) in observations and model
647 simulations support our hypothesis.
648

649 The difference of $p\text{CO}_2$ between SW and SWR was much lower than the difference of $p\text{CO}_2$ in
650 brine between the Arctic Ocean and the Southern Ocean. However, if we have added more
651 labile DOC instead of humic-rich riverine water to our mesocosms and if we extended the
652 duration of the experiment with lower air temperature, we may have observed larger differences
653 of DIC and $p\text{CO}_2$, closer to those observed in natural conditions. The availability of more labile
654 autochthonous DOC may promote higher bacterial respiration and higher accumulation of CO_2
655 in ice. Further, extending the duration of the experiment to several months, with further
656 decrease of the ice temperature, would increase the respiration burden, reduce the ice
657 permeability, and therefore reduce gases and DIC losses through the ice.

658 Because the addition of riverine DOC to seawater causes larger $p\text{CO}_2$ in ice, the Arctic Ocean,
659 which receives a large input of terrestrial DOC through rivers, might induce more positive (or
660 less negative) ice-air CO_2 fluxes than the Southern Ocean, for the same environmental
661 conditions. Similarly, Arctic coastal waters might also be associated with a more positive (or
662 negative) ice-air CO_2 fluxes than the central Arctic. This is at least true for the ice growth period
663 when algal growth is limited, as considered by the absence of autochthonous DOC in our
664 experiment. Algal growth would consume CO_2 but will also produce labile autochthonous DOC
665 that enhances bacterial production. Further experiments are therefore needed to refine the net
666 impact of algal and bacterial growth on $p\text{CO}_2$ in ice and on the inter-hemispheric differences.

667 The inter-hemispheric difference of $p\text{CO}_2$ in ice and brine likely results from the impact of ice
668 temperature on the ice permeability and the buffering effect of the carbonate system, in addition
669 to the DOC input. Lower ice temperatures are associated with larger buffering effects, i.e., the
670 increase of $p\text{CO}_2$ in the ice interior in response to a given increase of DIC (due to bacterial
671 respiration) would be enhanced. If the ice temperature is low enough so that the ice becomes
672 impermeable to gas exchange, the accumulation of $p\text{CO}_2$ would have been more obvious,
673 resulting in the larger observed inter-hemispheric difference of $p\text{CO}_2$ in ice and brine. On the
674 contrary, higher ice temperatures are associated with lower buffering effects and larger ice

675 permeability. Exchange may occur through the ice, and offset the bacterial accumulation of
676 CO₂. In our study, the impact of bacterial respiration on pCO₂ was most obvious in the ice
677 interior, because ice-air gas exchange and brine convection have offset the increase of pCO₂
678 associated with bacterial respiration at the ice interfaces.

679 Considering the drastic decline in Arctic sea ice, we may also wonder how air-sea and air-ice
680 CO₂ fluxes may change in the future. If the ice cover is replaced more and more by open water,
681 the most common scenario is that air-sea CO₂ fluxes increase, because gas exchange is more
682 efficient via an open sea surface than a semi-permeable ice cover. Our work highlighted the
683 fact that the dynamics regulating the pCO₂ gradient will be different too. Due to the buffering
684 effect of the carbonate system, brine concentration makes the pCO₂ more sensitive to DIC
685 increase in ice than in seawater, and a small accumulation of DIC, due to low bacterial
686 respiration may result in a large increase of pCO₂ in the ice. At some specific locations, where
687 bacterial activity is more intense in the ice than in the underlying water, the consequence of
688 bacterial respiration on pCO₂ in ice may be even more significant, especially when algal activity
689 is limited. The interplay between gas transfer velocity and the pCO₂ gradient needs to be taken
690 into consideration while assessing the future evolution of the air-sea and air-ice CO₂ fluxes in
691 the polar regions.

692

693 **Acknowledgments**

694 We are grateful to two anonymous reviewers for their useful comments which have improved
695 the quality of the manuscript. This study was supported by the European Community's 7th
696 Framework Programme through the grant to the budget of the Integrated Infrastructure
697 Initiative HYDRALAB-IV, Contract no. 261520. The authors would like to thank the Hamburg
698 Ship Model Basin (HSVA), Karl-Ulrich Evers and the rest of the ice tank crew, for the
699 hospitality, technical and scientific support and the professional execution of the test program
700 in the Research Infrastructure ARCTICLAB. The work was supported by a FiDiPro award by
701 the Academy of Finland, the Walter and Andree Nottbeck Foundation, and the BIGSOUTH
702 project funded by the Belgian Science Federal Policy Office. MK, SM and BD are respectively
703 research fellows, postdoctoral researcher and research associate of the Fonds de la Recherche
704 Scientifique –FNRS. JZ was a F.R.S.-FNRS research fellow and is presently a BAEF Francqui
705 Foundation research fellow. This is a MARE contribution n°XXX.

706

707 **Contributions**

708 JLT, BD, GD, HK, GK planned and designed the experiment under the lead of DT; JZ, MK,
709 JLT, BD, GD and DT provided the data on sea ice physics and carbonate chemistry, HK, the
710 bacterial data, GK, the DOC data, and SM, the model simulations. JZ, BD, HK, SM wrote the
711 paper with the valuable comments and inputs from all the other co-authors.

712

713 Captions

714 Figure 1. pCO₂ measurements in sea ice and brine in the Arctic and Antarctica after Geilfus et
715 al. (2014), excluding the measurements where flooding was observed. The horizontal line
716 indicates a pCO₂ of 400ppm - a reference value considering current atmospheric pCO₂.

717 Figure 2. Brine volume fraction (BrV, in %) and Rayleigh number (Ra) in the SW and SWR
718 mesocosms during the experiment. The black dots are the data points from the sampling, while
719 the color in between results is from interpolation (natural neighbours in Surfer 8 © software)
720 (Zhou et al., 2014).

721 Figure 3. a) Bacterial respiration (BR_TdR), b) DIC₇ and c) pCO₂ in water and sea ice. Note
722 that for sea ice, we plotted the median value of each ice core.

723 Figure 4. Bacterial respiration (BR_TdR) in ice in the SW and SWR mesocosms during the
724 experiment, and the difference between both mesocosms. Bacterial respiration is expressed in
725 nmol C L⁻¹ h⁻¹.

726 Figure 5. DIC₇ in ice of the SW and SWR mesocosms during the experiment, and the difference
727 between both mesocosms. DIC₇ is expressed in μmol C kg⁻¹. Insignificant differences of DIC₇
728 are set in white.

729 Figure 6. pCO₂ in ice in the SW and SWR mesocosms during the experiment, and the difference
730 between both mesocosms. pCO₂ is expressed in ppm. Insignificant differences of pCO₂ are set
731 in white.

732 Figure 7. Relationship between pCO₂ in ice and brine volume fraction. The circles are the data
733 used to draw the fit (black curve), the other discrete symbols are not considered (see explanation
734 in the text). The blue curves are the 95 % confidence bands of the fit and the red dashed curve
735 is the relationship predicted by CO2SYS (Lewis and Wallace, 1998).

736 Figure 8. Buffer factor of the carbonate system for decreasing temperature and related increase
737 of salinity due to brine concentration/dilution in a closed system. Initial conditions was S =
738 35.17, T = -1.8 °C, TA = 2578 μmol kg⁻¹, DIC = 2450.4 μmol kg⁻¹, pCO₂ = 400 μatm. β is
739 provided for an increase of DIC of 20 μmol kg⁻¹.

740 Figure 9. (Clockwise) Temporal changes of the ice thickness, median ice temperature, median
741 ice salinity, the standing stock of DIC and the median pCO₂ in the ice. The dots refer to the
742 measurements (white for SW and black for SWR), while the curves refer to the simulated
743 results. The vertical dashed line shows the transition from ice growth to ice decay.

744 Figure 10 Modeled DIC₇ in ice, in SW and SWR mesocosms, and the difference SWR minus
745 SW, using a median bacterial respiration in ice associated with a BGE of 0.15 (Table 1).

746 Figure 11. Modeled pCO₂ in ice, in SW and SWR mesocosms, and the difference SWR minus
747 SW, using a median bacterial respiration in ice associated with a BGE of 0.15 (Table 1).

748 Table 1. Calculated median bacterial respiration (BR) in ice in SW and SWR using different
749 bacterial growth efficiencies (BGE), the measured median difference of pCO₂ and DIC (SWR
750 minus SW) during the experiment (Diff pCO₂ and Diff DIC₇), and the modeled difference of
751 pCO₂ and DIC for each set of BGE-dependent BR.

752

753 **References**

- 754 Anderson, G.M., 1976. Error propagation by the Monte Carlo method in geochemical
755 calculations. *Geochim. Cosmochim. Acta* 40, 1533–1538.
- 756 Aslam, S.N., Underwood, G.J.C., Kaartokallio, H., Norman, L., Autio, R., Fischer, M.,
757 Kuosa, H., Dieckmann, G.S., Thomas, D.N., 2012. Dissolved extracellular polymeric
758 substances (dEPS) dynamics and bacterial growth during sea ice formation in an ice tank
759 study. *Polar Biol.* 35, 661–676. doi:10.1007/s00300-011-1112-0
- 760 Baer, S., Connelly, T., Bronk, D., 2015. Nitrogen uptake dynamics in landfast sea ice of the
761 Chukchi Sea. *Polar Biol.* 38, 781–797. doi:10.1007/s00300-014-1639-y
- 762 Brown, K.A., Miller, L.A., Davelaar, M., Francois, R., Tortell, P.D., 2014. Over-
763 determination of the carbonate system in natural sea-ice brine and assessment of
764 carbonic acid dissociation constants under low temperature, high salinity conditions.
765 *Mar. Chem.* 165, 36–45. doi:10.1016/j.marchem.2014.07.005
- 766 Copin-Montegut, C., 1988. A new formula for the effect of temperature on the partial pressure
767 of CO₂ in seawater. *Mar. Chem.* 25, 29–37. doi:10.1016/0304-4203(88)90012-6
- 768 Cox, G.F.N., Weeks, W.F., 1983. Equations for determining the gas and brine volumes in sea
769 ice samples. *J. Glaciol.* 29, 306–316.
- 770 Crabeck, O., Delille, B., Thomas, D., Geilfus, N.-X., Rysgaard, S., Tison, J.-L., 2014. CO₂
771 and CH₄ in sea ice from a subarctic fjord under influence of riverine input.
772 *Biogeosciences* 11, 6525–6538. doi:10.5194/bg-11-6525-2014
- 773 Del Giorgio, P., Cole, J.J., 1998. Bacterial growth efficiency in natural aquatic systems.
774 *Annu. Rev. Ecol. Syst.* 29, 503–541.
- 775 Delille, B., 2006. Inorganic carbon dynamics and air-ice-sea CO₂ fluxes in the open and
776 coastal waters of the Southern Ocean. Université de Liège, Belgique.
- 777 Delille, B., Harlay, J., Zondervan, I., Jacquet, S., Chou, L., Wollast, R., Bellerby, R.G.J.,
778 Frankignoulle, M., Borges, A.V., Riebesell, U., Gattuso, J.P., 2005. Response of primary
779 production and calcification to changes of pCO₂ during experimental blooms of the
780 coccolithophorid *Emiliana huxleyi*. *Global Biogeochem. Cycles* 19, 1–14.
781 doi:10.1029/2004GB002318
- 782 Delille, B., Jourdain, B., Borges, A. V., Tison, J.-L., Delille, D., 2007. Biogas (CO₂, O₂,
783 dimethylsulfide) dynamics in spring Antarctic fast ice. *Limnol. Oceanogr.* 52, 1367–
784 1379. doi:10.4319/lo.2007.52.4.1367
- 785 Delille, B., Vancoppenolle, M., Geilfus, N.-X., Tilbrook, B., Lannuzel, D., Schoemann, V.,
786 Becquevort, S., Carnat, G., Delille, D., Lancelot, C., Chou, L., Dieckmann, G.S., Tison,
787 J.-L., 2014. Southern Ocean CO₂ sink: The contribution of the sea ice. *J. Geophys. Res.*
788 *Ocean.* 119, 6340–6355. doi:10.1002/2014JC009941

- 789 Dickson, A.G., Millero, F.J., 1987. A comparison of the equilibrium constants for the
790 dissociation of carbonic acid in seawater media. *Deep Sea Res.* 34, 1733–1743.
791 doi:10.1016/0198-0149(87)90021-5
- 792 Dieckmann, G.S., Nehrke, G., Papadimitriou, S., Göttlicher, J., Steininger, R., Kennedy, H.,
793 Wolf-Gladrow, D., Thomas, D.N., 2008. Calcium carbonate as ikaite crystals in
794 Antarctic sea ice. *Geophys. Res. Lett.* 35, 35–37. doi:10.1029/2008GL033540
- 795 Dieckmann, G.S., Nehrke, G., Uhlig, C., Göttlicher, J., Gerland, S., Granskog, M.A., Thomas,
796 D.N., 2010. Brief Communication: Ikaite (CaCO₃·6H₂O) discovered in Arctic sea ice.
797 *Cryosphere* 4, 227–230. doi:10.5194/tc-4-227-2010
- 798 Dittmar, T., Kattner, G., 2003. The biogeochemistry of the river and shelf ecosystem of the
799 Arctic Ocean: a review. *Mar. Chem.* 83, 103–120. doi:10.1016/S0304-4203(03)00105-1
- 800 DOE, 1994. Handbook of Methods for the Analysis of the Various Parameters of the Carbon
801 Dioxide System in Sea Water; version2.
- 802 Eronen-Rasimus, E., Kaartokallio, H., Lyra, C., Autio, R., Kuosa, H., Dieckmann, G.S.,
803 Thomas, D.N., 2014. Bacterial community dynamics and activity in relation to dissolved
804 organic matter availability during sea-ice formation in a mesocosm experiment.
805 *Microbiologyopen* 3, 139–156. doi:10.1002/mbo3.157
- 806 Frankignoulle, M., 1994. A complete set of buffer factors for acid/base CO₂ system in
807 seawater. *J. Mar. Syst.* 5, 111–118. doi:10.1016/0924-7963(94)90026-4
- 808 Fuhrman, J.A., Azam, F., 1982. Thymidine incorporation as a measure of heterotrophic
809 bacterioplankton production in marine surface waters: Evaluation and field results. *Mar.*
810 *Biol.* 66, 109–120. doi:10.1007/BF00397184
- 811 Fuhrman, J.A., Azam, F., 1980. Bacterioplankton secondary production estimates for coastal
812 waters of British Columbia, Antarctica, and California. *Appl. Environ. Microbiol.* 39,
813 1085–1095.
- 814 Geilfus, N.-X., Carnat, G., Dieckmann, G.S., Halden, N., Nehrke, G., Papakyriakou, T.,
815 Tison, J.-L., Delille, B., 2013. First estimates of the contribution of CaCO₃ precipitation
816 to the release of CO₂ to the atmosphere during young sea ice growth. *J. Geophys. Res.*
817 *Ocean.* 118, 244–255. doi:10.1029/2012JC007980
- 818 Geilfus, N.-X., Carnat, G., Papakyriakou, T., Tison, J.-L., Else, B., Thomas, H., Shadwick, E.,
819 Delille, B., 2012a. Dynamics of pCO₂ and related air-ice CO₂ fluxes in the Arctic
820 coastal zone (Amundsen Gulf, Beaufort Sea). *J. Geophys. Res. Ocean.* 117, C00G10.
821 doi:10.1029/2011JC007118
- 822 Geilfus, N.-X., Delille, B., Verbeke, V., Tison, J.-L., 2012b. Towards a method for high
823 vertical resolution measurements of the partial pressure of CO₂ within bulk sea ice. *J.*
824 *Glaciol.* 58, 287–300. doi:10.3189/2012JoG11J071
- 825 Geilfus, N.-X., Tison, J.-L., Ackley, S.F., Galley, R.J., Rysgaard, S., Miller, L.A., Delille, B.,
826 2014. Sea ice pCO₂ dynamics and air-ice CO₂ fluxes during the Sea Ice Mass Balance in

- 827 the Antarctic (SIMBA) experiment – Bellingshausen Sea, Antarctica. *Cryosph.* 8, 2395–
828 2407. doi:10.5194/tc-8-2395-2014
- 829 Giannelli, V., Thomas, D.N., Haas, C., Kattner, G., Kennedy, H., Dieckmann, G.S., 2001.
830 Behaviour of dissolved organic matter and inorganic nutrients during experimental sea-
831 ice formation. *Ann. Glaciol.* 33, 317–321. doi:10.3189/172756401781818572
- 832 Golden, K.M., Ackley, S.F., Lytle, V.I., 1998. The percolation phase transition in sea ice.
833 *Science* (80-.). 282, 2238–2241. doi:10.1126/science.282.5397.2238
- 834 Gosink, T.A., Pearson, J.G., Kelley, J.J., 1976. Gas movement through sea ice. *Nature* 263,
835 41–42.
- 836 Goyet, C., Poisson, A., 1989. New determination of carbonic acid dissociation constants in
837 seawater as a function of temperature and salinity. *Deep Sea Res.* 36, 1635–1654.
838 doi:10.1016/0198-0149(89)90064-2
- 839 Gran, G., 1952. Determination of the Equivalence Point in Potentiometric Titrations. Part II.
840 *Analyst* 77, 661–671.
- 841 Hansell, D., Carlson, C., Repeta, D., Schlitzer, R., 2009. Dissolved Organic Matter in the
842 Ocean: A Controversy Stimulates New Insights. *Oceanography*.
843 doi:10.5670/oceanog.2009.109
- 844 Helmke, E., Weyland, H., 1995. Bacteria in sea ice and underlying water of the eastern
845 Weddell Sea in midwinter. *Mar. Ecol. Prog. Ser.* 117, 269–288.
846 doi:10.3354/meps117269
- 847 Hunke, E.C., Notz, D., Turner, A.K., Vancoppenolle, M., 2011. The multiphase physics of sea
848 ice: a review for model developers. *Cryosph.* 5, 989–1009. doi:10.5194/tc-5-989-2011
- 849 Jørgensen, L., Stedmon, C. a., Kaartokallio, H., Middelboe, M., Thomas, D.N., 2015.
850 Changes in the composition and bioavailability of dissolved organic matter during sea
851 ice formation. *Limnol. Oceanogr.* 00, 00–00. doi:10.1002/lno.10058
- 852 Kaartokallio, H., 2004. Food web components, and physical and chemical properties of Baltic
853 Sea ice. *Mar. Ecol. Prog. Ser.* 273, 49–63. doi:10.3354/meps273049
- 854 Kirchman, D.L., Hill, V., Cottrell, M.T., Gradinger, R., Malmstrom, R.R., Parker, A., 2009.
855 Standing stocks, production, and respiration of phytoplankton and heterotrophic bacteria
856 in the western Arctic Ocean. *Deep. Res. Part II Top. Stud. Oceanogr.* 56, 1237–1248.
857 doi:10.1016/j.dsr2.2008.10.018
- 858 Kotovitch, M., Moreau, S., Zhou, J., Goosse, H., Vancoppenolle, M., Dieckmann, G.S.,
859 Thomas, D.N., Tison, J.-L., Delille, B., n.d. Measurements of air-ice CO₂ fluxes over
860 experimental sea ice emphasize the role of bubbles in gas transport during ice growth,
861 *Elementa: Science of the Anthropocene*.

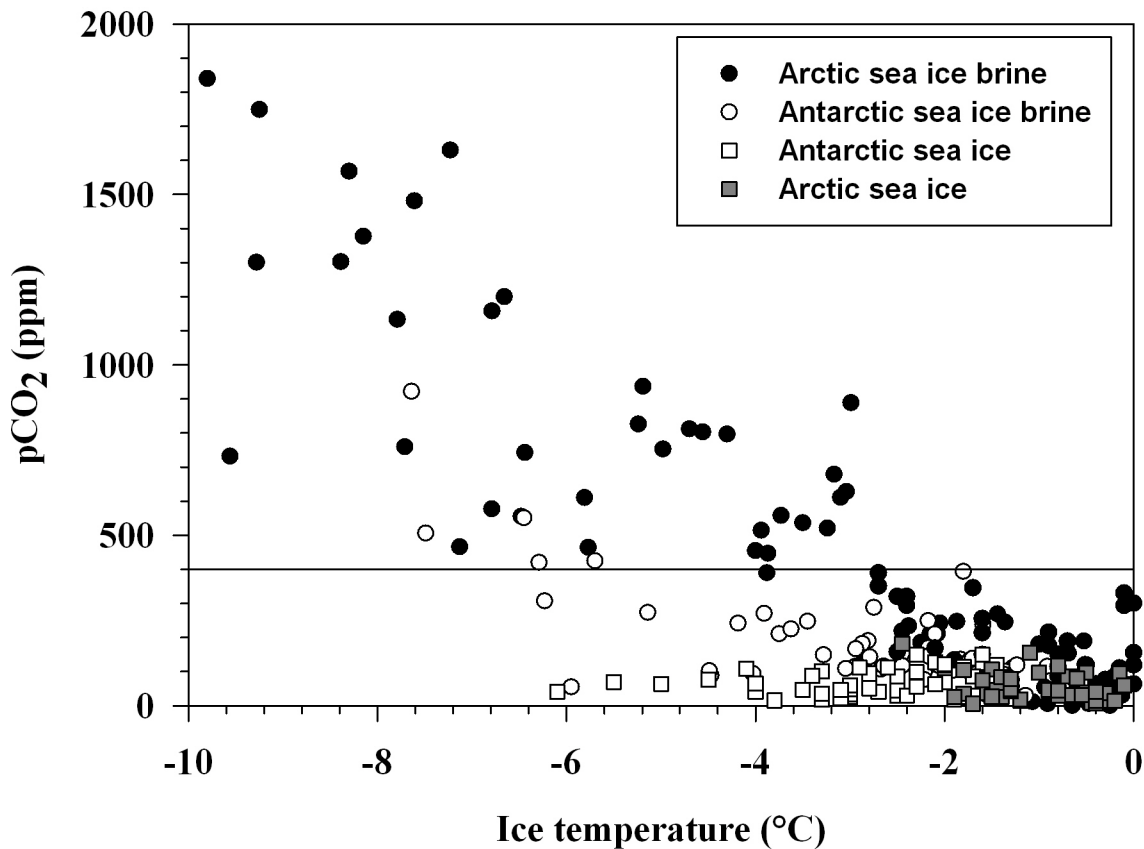
- 862 Krembs, C., Eicken, H., Deming, J.W., 2011. Exopolymer alteration of physical properties of
863 sea ice and implications for ice habitability and biogeochemistry in a warmer Arctic.
864 Proc. Natl. Acad. Sci. U. S. A. 108, 3653–8. doi:10.1073/pnas.1100701108
- 865 Kuparinen, J., Autio, R., Kaartokallio, H., 2011. Sea ice bacterial growth rate, growth
866 efficiency and preference for inorganic nitrogen sources in the Baltic Sea. Polar Biol. 34,
867 1361–1373. doi:10.1007/s00300-011-0989-y
- 868 Lewis, E., Wallace, D.W.R., 1998. Program developed for CO₂ system calculations.
- 869 Loose, B., McGillis, W.R., Perovich, D., Zappa, C.J., Schlosser, P., 2014. A parameter model
870 of gas exchange for the seasonal sea ice zone. Ocean Sci. 10, 17–28. doi:10.5194/os-10-
871 17-2014
- 872 Loose, B., Schlosser, P., Perovich, D., Ringelberg, D., Ho, D.T., Takahashi, T., Richter-
873 Menge, J., Reynolds, C.M., McGillis, W.R., Tison, J.-L., 2011. Gas diffusion through
874 columnar laboratory sea ice: implications for mixed-layer ventilation of CO₂ in the
875 seasonal ice zone. Tellus B 63, 23–39. doi:10.1111/j.1600-0889.2010.00506.x
- 876 Marion, G.M., 2001. Carbonate mineral solubility at low temperatures in the Na-K-Mg-Ca-H-
877 Cl-SO₄-OH-HCO₃-CO₃-CO₂-H₂O system. Geochim. Cosmochim. Acta 65, 1883–
878 1896.
- 879 Mehrbach, C., Culbrton, C.H., Hawley, J.E., Pytkowicz, R.M., 1973. Measurement of the
880 apparent dissociation constants of carbonic acid in seawater at atmospheric pressure.
881 Limnol. Oceanogr. 18, 897–907. doi:10.4319/lo.1973.18.6.0897
- 882 Miller, L.A., Carnat, G., Else, B.G.T., Sutherland, N., Papakyriakou, T.N., 2011a. Carbonate
883 system evolution at the Arctic Ocean surface during autumn freeze-up. J. Geophys. Res.
884 116, C00G04. doi:10.1029/2011JC007143
- 885 Miller, L.A., Papakyriakou, T.N., Collins, R.E., Deming, J.W., Ehn, J.K., Macdonald, R.W.,
886 Mucci, A., Owens, O., Raudsepp, M., Sutherland, N., 2011b. Carbon dynamics in sea
887 ice: A winter flux time series. J. Geophys. Res. 116, C02028.
888 doi:10.1029/2009JC006058
- 889 Moreau, S., Kaartokallio, H., Vancoppenolle, M., Zhou, J., Kotovitch, M., Dieckmann, G.S.,
890 Thomas, D.N., Goosse, H., Tison, J.-L., Delille, B., n.d. Closing the O₂ and CO₂ budget
891 under a growing ice sheet - a laboratory investigation, Elementa: Science of the
892 Anthropocene.
- 893 Moreau, S., Vancoppenolle, M., Delille, B., Tison, J.-L., Zhou, J., Kotovitch, M., Thomas,
894 D.N., Geilfus, N.-X., Goosse, H., 2015. Drivers of inorganic carbon dynamics in first-
895 year sea ice: A model study. J. Geophys. Res. Ocean. 120, 471–495.
896 doi:10.1002/2014JC010388
- 897 Moreau, S., Vancoppenolle, M., Zhou, J., Tison, J.-L., Delille, B., Goosse, H., 2014.
898 Modelling argon dynamics in first-year sea ice. Ocean Model. 73, 1–18.
899 doi:10.1016/j.ocemod.2013.10.004

- 900 Müller, S., Vähätalo, A. V., Stedmon, C. a., Granskog, M. a., Norman, L., Aslam, S.N.,
 901 Underwood, G.J.C., Dieckmann, G.S., Thomas, D.N., 2013. Selective incorporation of
 902 dissolved organic matter (DOM) during sea ice formation. *Mar. Chem.* 155, 148–157.
 903 doi:10.1016/j.marchem.2013.06.008
- 904 Nagata, T., Watanabe, Y., 1990. Carbon- and nitrogen-to-volume ratios of bacterioplankton
 905 grown under different nutritional conditions. *Appl. Environ. Microbiol.* 56, 1303–1309.
- 906 Nguyen, D., Maranger, R., 2011. Respiration and bacterial carbon dynamics in Arctic sea ice.
 907 *Polar Biol.* 34, 1843–1855. doi:10.1007/s00300-011-1040-z
- 908 Nguyen, D., Maranger, R., Tremblay, J.É., Gosselin, M., 2012. Respiration and bacterial
 909 carbon dynamics in the Amundsen Gulf, western Canadian Arctic. *J. Geophys. Res.*
 910 *Ocean.* 117, 1–12. doi:10.1029/2011JC007343
- 911 Nomura, D., Eicken, H., Gradinger, R., Shirasawa, K., 2010. Rapid physically driven
 912 inversion of the air–sea ice CO₂ flux in the seasonal landfast ice off Barrow, Alaska after
 913 onset of surface melt. *Cont. Shelf Res.* 30, 1998–2004. doi:10.1016/j.csr.2010.09.014
- 914 Notz, D., Worster, M.G., 2009. Desalination processes of sea ice revisited. *J. Geophys. Res.*
 915 114, C05006. doi:10.1029/2008JC004885
- 916 Notz, D., Worster, M.G., 2008. In situ measurements of the evolution of young sea ice. *J.*
 917 *Geophys. Res. Ocean.* 113, C03001. doi:10.1029/2007JC004333
- 918 Papadimitriou, S., Thomas, D.N., Kennedy, H., Haas, C., Kuosa, H., Krell, A., Dieckmann,
 919 G.S., 2007. Biogeochemical composition of natural sea ice brines from the Weddell Sea
 920 during early austral summer. *Limnol. Oceanogr.* 52, 1809–1823.
 921 doi:10.4319/lo.2007.52.5.1809
- 922 Pelegrí, S.P., Dolan, J., Rassoulzadegan, F., 1999. Use of high temperature catalytic oxidation
 923 (HTCO) to measure carbon content of microorganisms. *Aquat. Microb. Ecol.* 16, 273–
 924 280. doi:10.3354/ame016273
- 925 Rivkin, R.B., Legendre, L., 2001. Biogenic carbon cycling in the upper ocean: effects of
 926 microbial respiration. *Science* (80-.). 291, 2398–2400.
- 927 Rysgaard, S., Glud, R.N., Sejr, M.K., Bendtsen, J., Christensen, P.B., 2007. Inorganic carbon
 928 transport during sea ice growth and decay: A carbon pump in polar seas. *J. Geophys.*
 929 *Res.* 112, C03016. doi:10.1029/2006JC003572
- 930 Shadwick, E.H., Thomas, H., Chierici, M., Else, B., Fransson, A., Michel, C., Miller, L.A.,
 931 Mucci, A., Niemi, A., Papakyriakou, T.N., Tremblay, J.-É., 2011. Seasonal variability of
 932 the inorganic carbon system in the Amundsen Gulf region of the southeastern Beaufort
 933 Sea. *Limnol. Oceanogr.* 56, 303–322. doi:10.4319/lo.2011.56.1.0303
- 934 Smith, R.E.H., Clement, P., 1990. Heterotrophic activity and bacterial productivity in
 935 assemblages of microbes from sea ice in the high Arctic. *Polar Biol.* 10, 351–357.
 936 doi:10.1007/BF00237822

- 937 Vancoppenolle, M., Goosse, H., de Montety, A., Fichefet, T., Tremblay, B., Tison, J.-L.,
938 2010. Modeling brine and nutrient dynamics in Antarctic sea ice: The case of dissolved
939 silica. *J. Geophys. Res.* 115, C02005. doi:10.1029/2009JC005369
- 940 Zhou, J., Delille, B., Eicken, H., Vancoppenolle, M., Brabant, F., Carnat, G., Geilfus, N.-X.,
941 Papakyriakou, T., Heinesch, B., Tison, J.-L., 2013. Physical and biogeochemical
942 properties in landfast sea ice (Barrow, Alaska): Insights on brine and gas dynamics
943 across seasons. *J. Geophys. Res. Ocean.* 118, 3172–3189. doi:10.1002/jgrc.20232
- 944 Zhou, J., Delille, B., Kaartokallio, H., Kattner, G., Kuosa, H., Tison, J.-L., Autio, R.,
945 Dieckmann, G.S., Evers, K.-U., Jørgensen, L., Kennedy, H., Kotovitch, M., Luhtanen,
946 A.-M., Stedmon, C.A., Thomas, D.N., 2014. Physical and bacterial controls on inorganic
947 nutrients and dissolved organic carbon during a sea ice growth and decay experiment.
948 *Mar. Chem.* 166, 59–69. doi:10.1016/j.marchem.2014.09.013
- 949
- 950
- 951
- 952

	Observations				Model	
	BR (SW)	BR (SWR)	Diff pCO₂	Diff DIC₇	Diff pCO₂	Diff DIC₇
	nmol C L ⁻¹ h ⁻¹	nmol C L ⁻¹ h ⁻¹	ppm	μmol kg ⁻¹	ppm	μmol kg ⁻¹
BGE = 0.348	10.0	24.7	13	2.8	8.3	0.9
BGE = 0.2	21.5	52.6			19.3	1.9
BGE = 0.15	30.4	74.6			31.9	2.7

Fig. 1



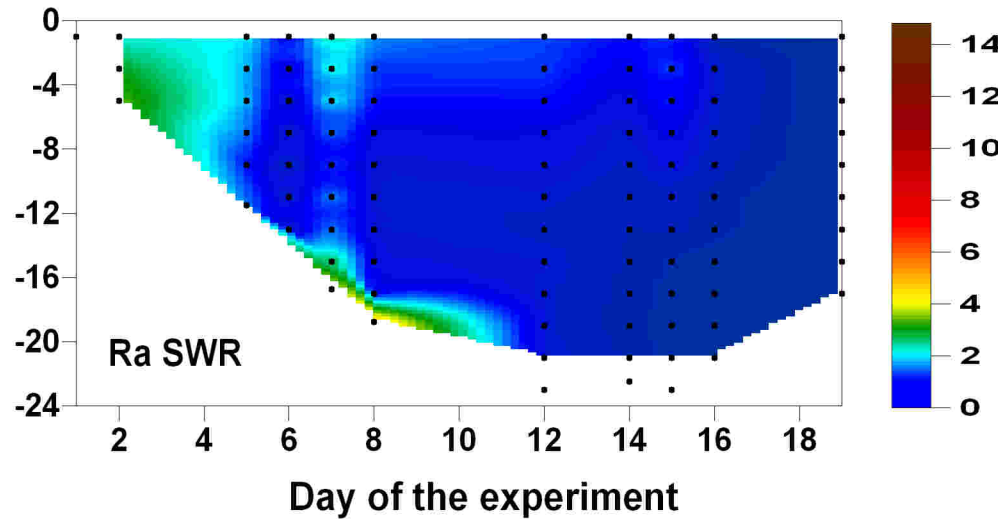
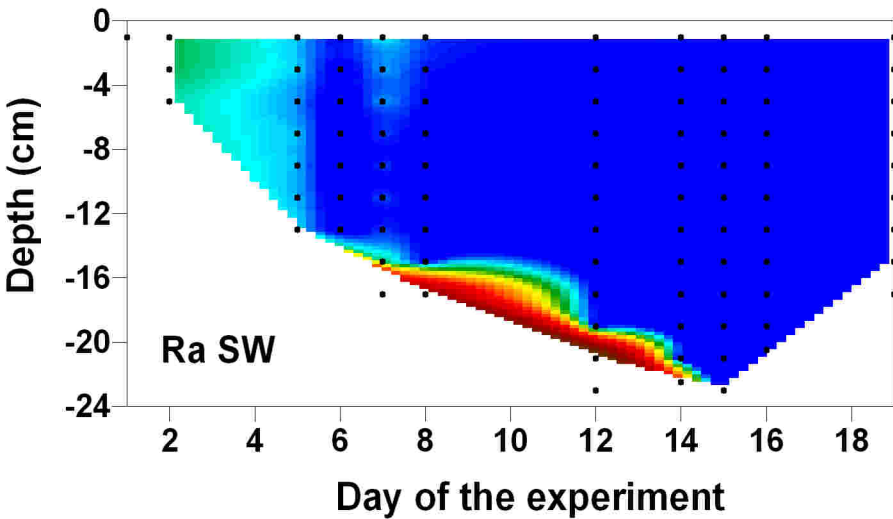
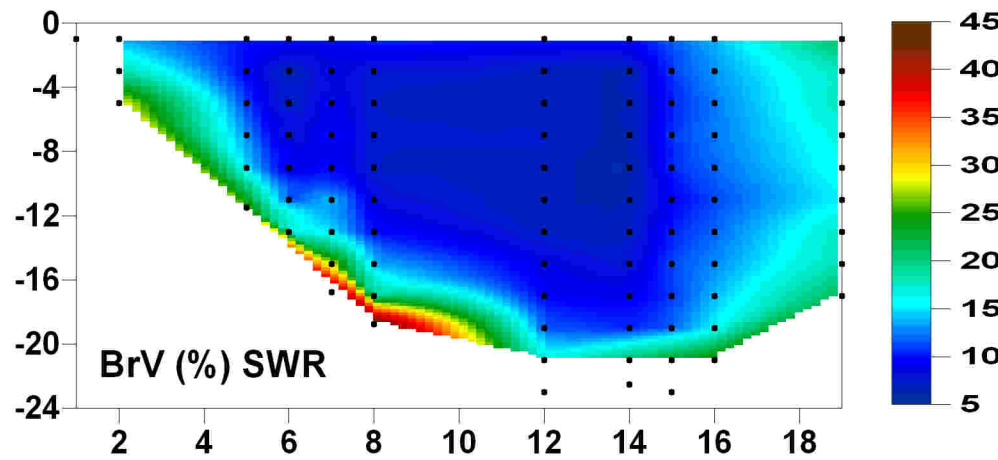
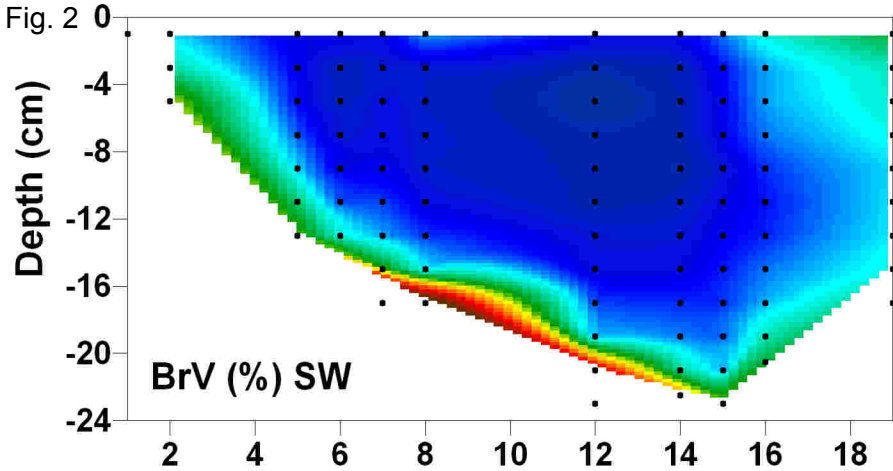
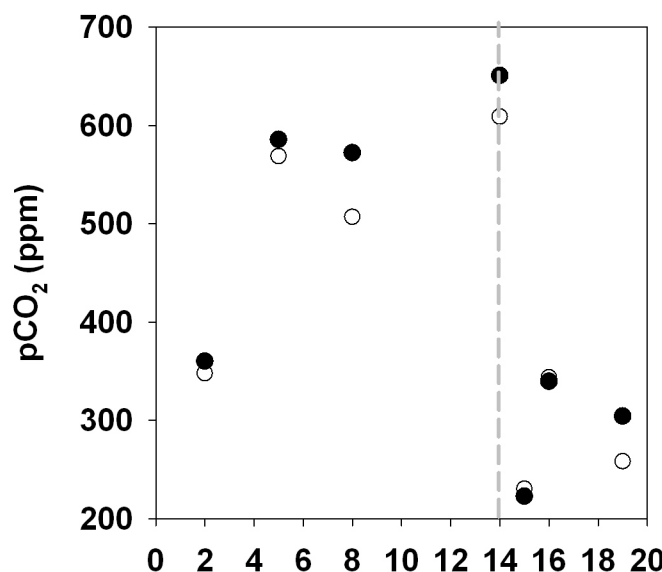
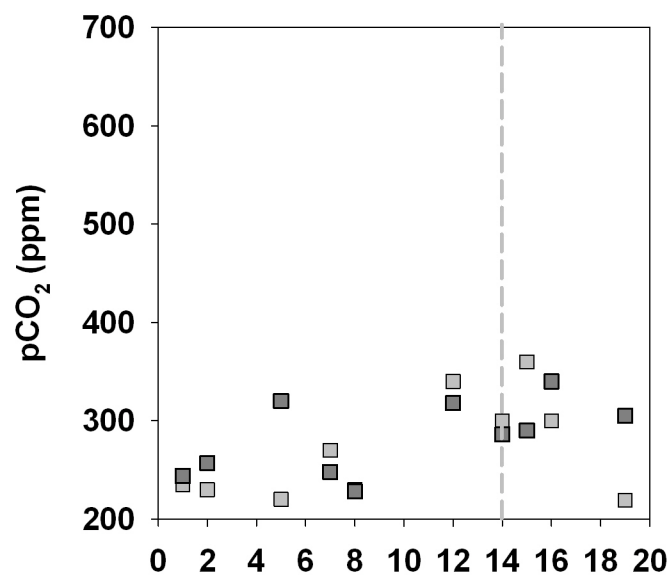
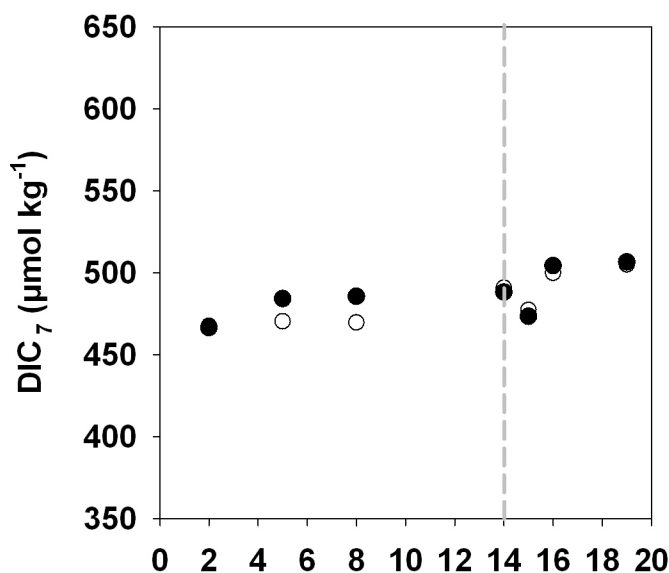
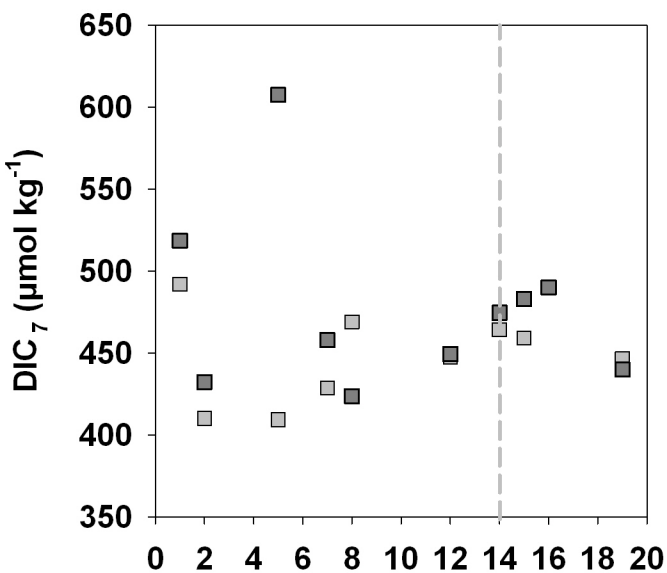
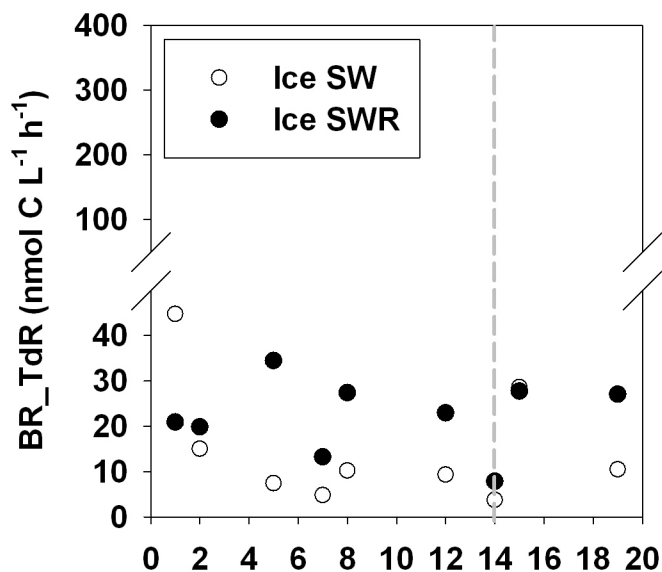
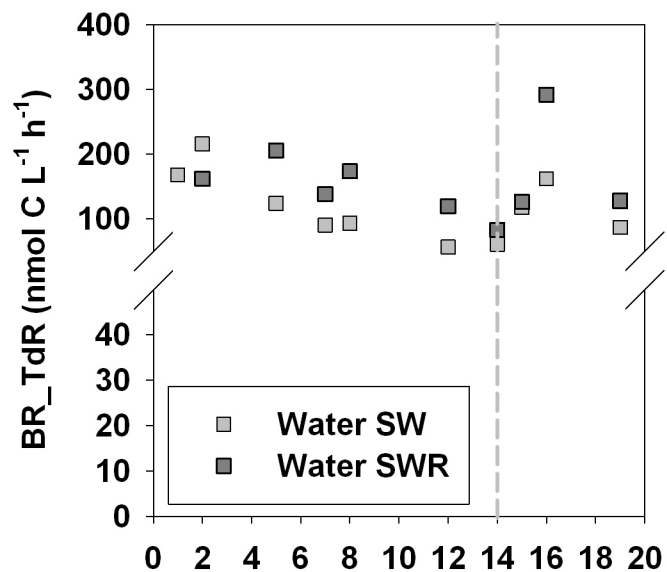


Fig.3



Day of the experiment

Day of the experiment

Fig. 4

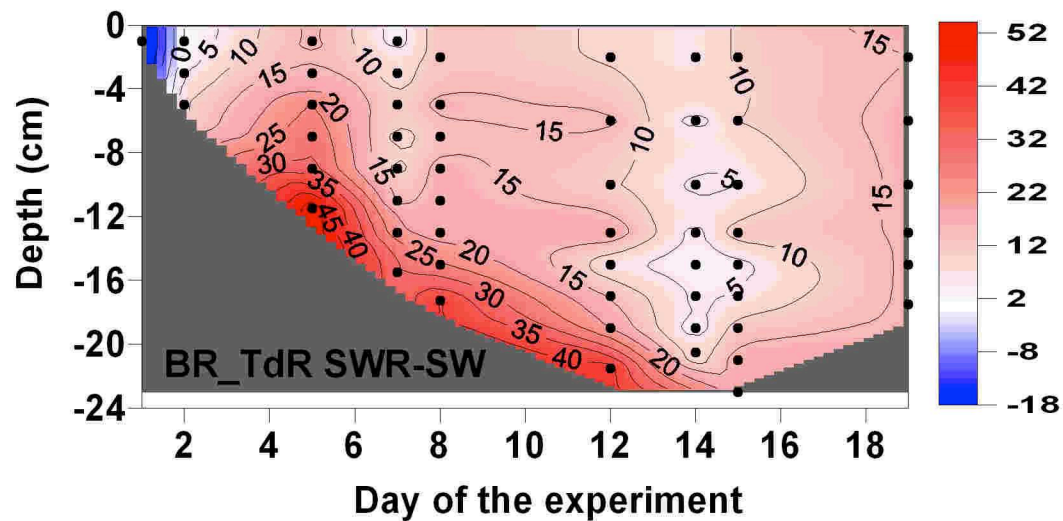
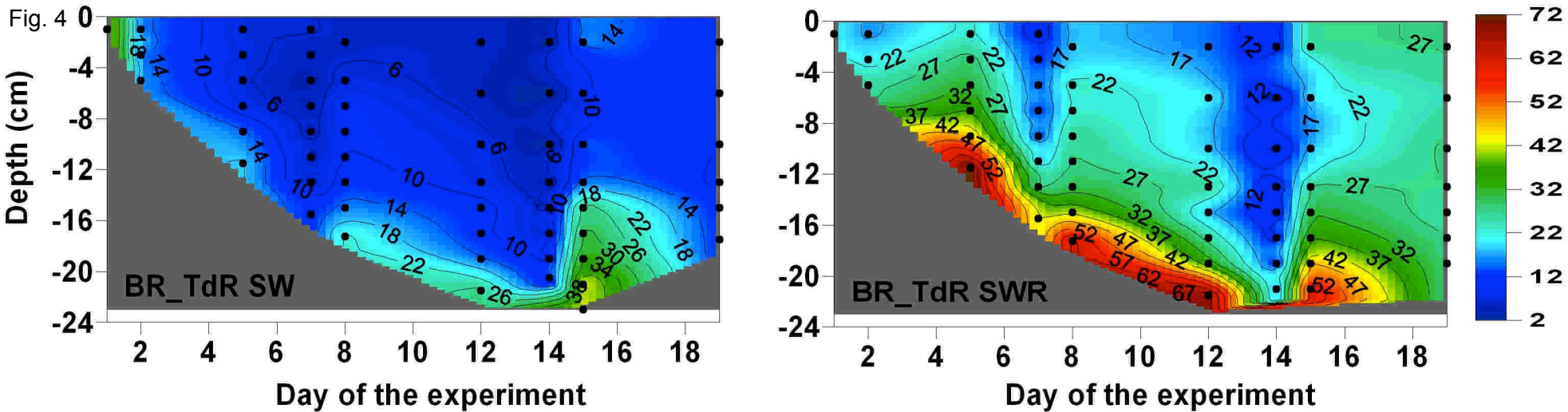
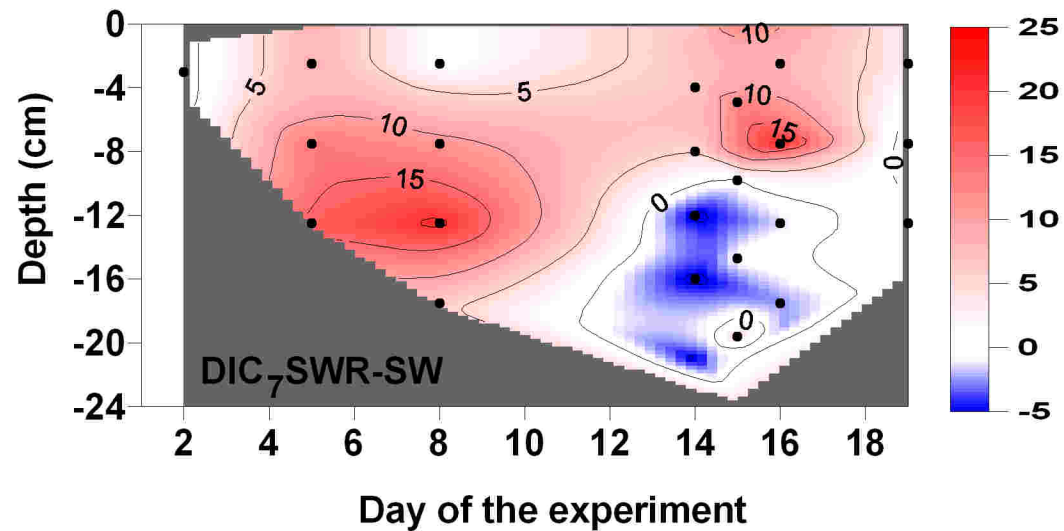
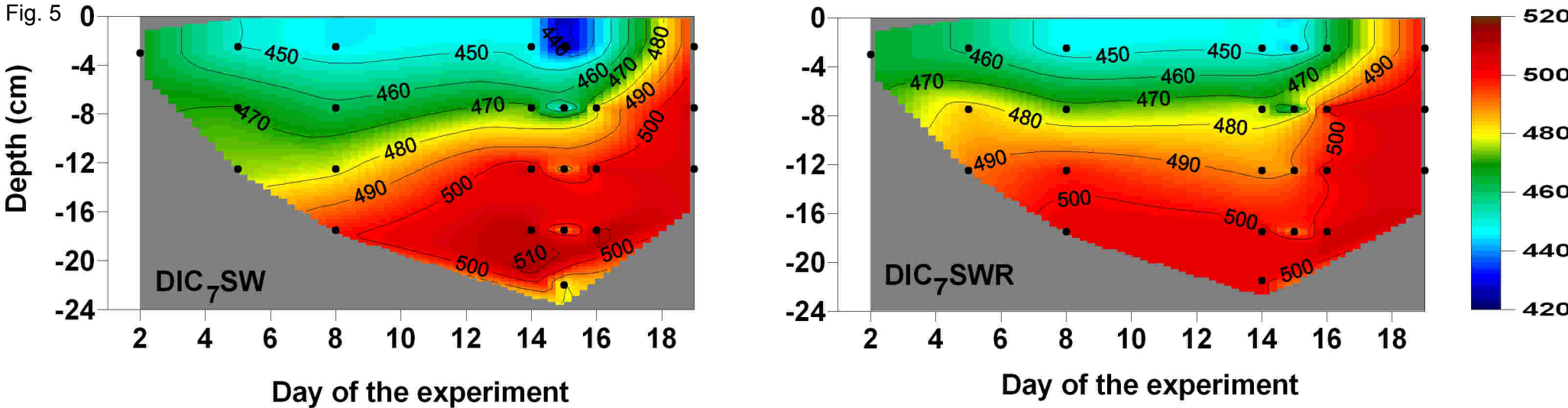


Fig. 5



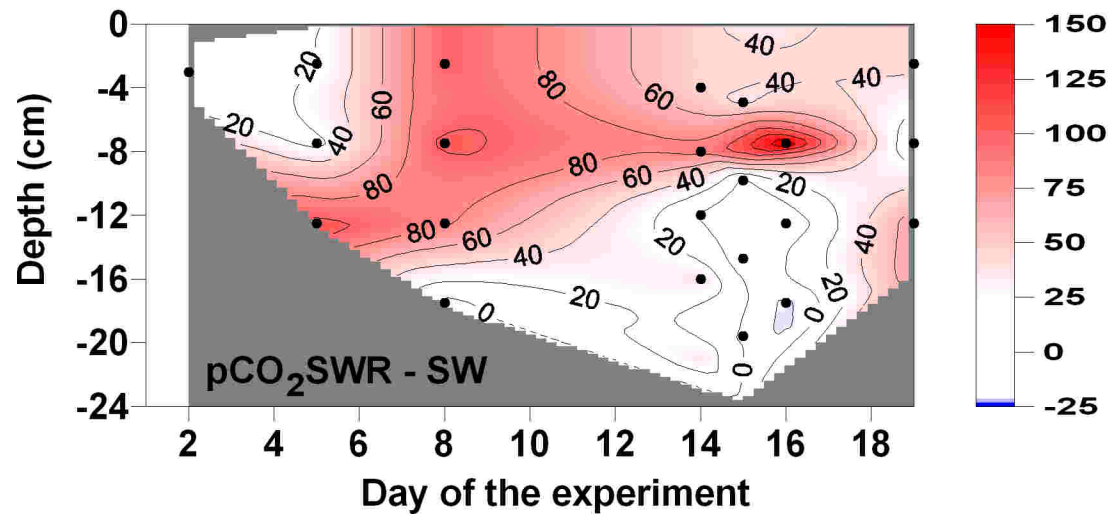
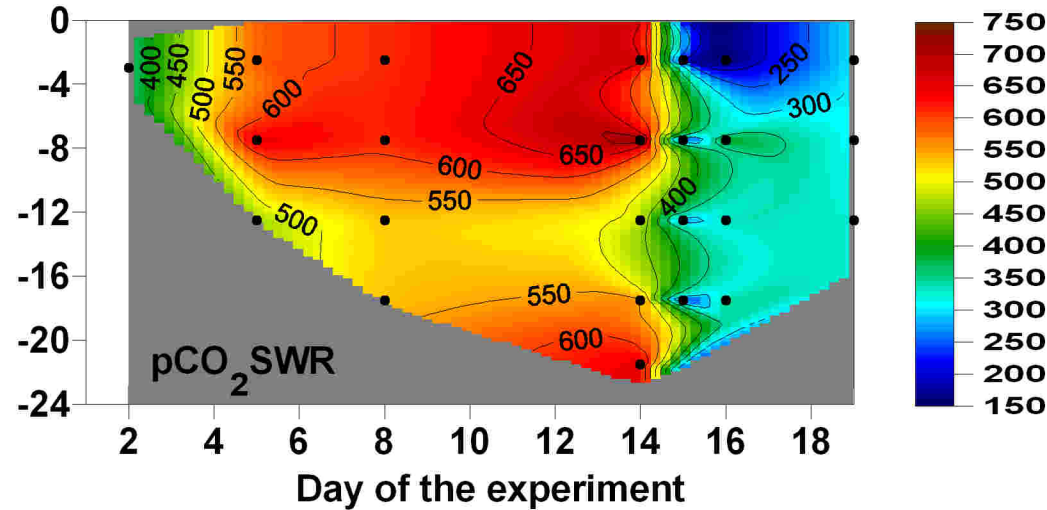
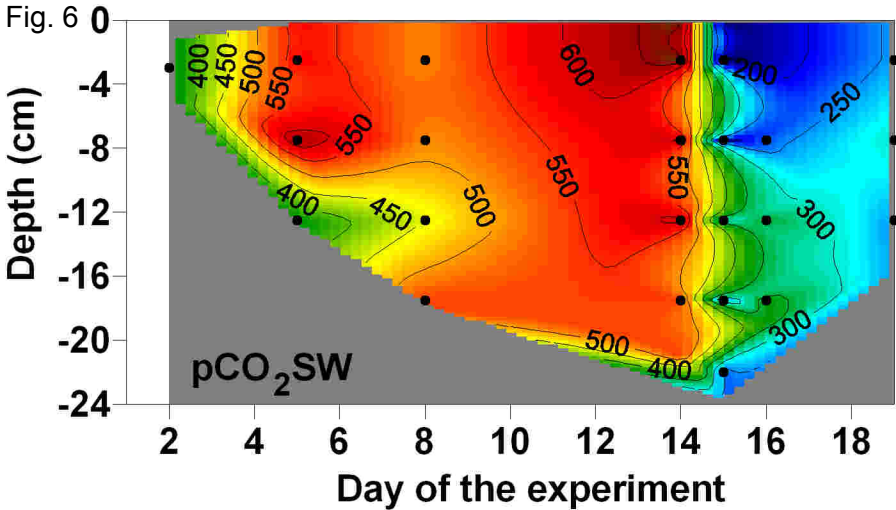


Fig. 7

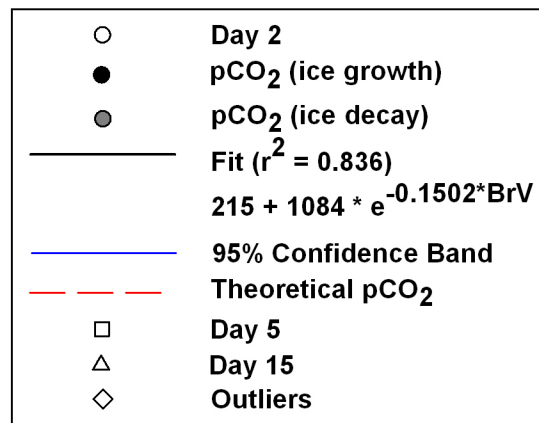
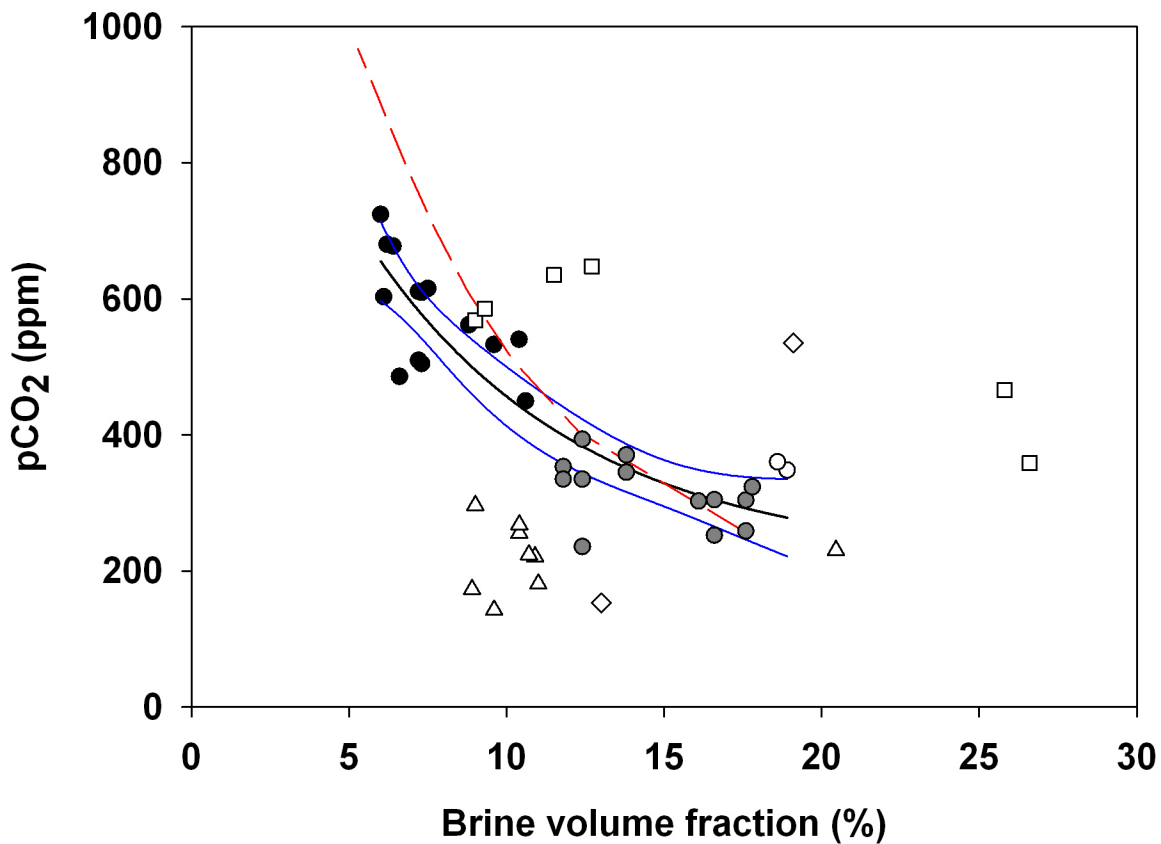


Fig. 8

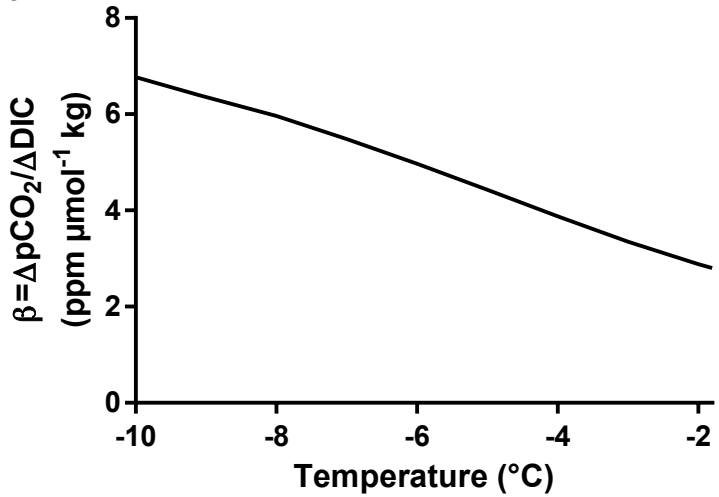


Fig. 9

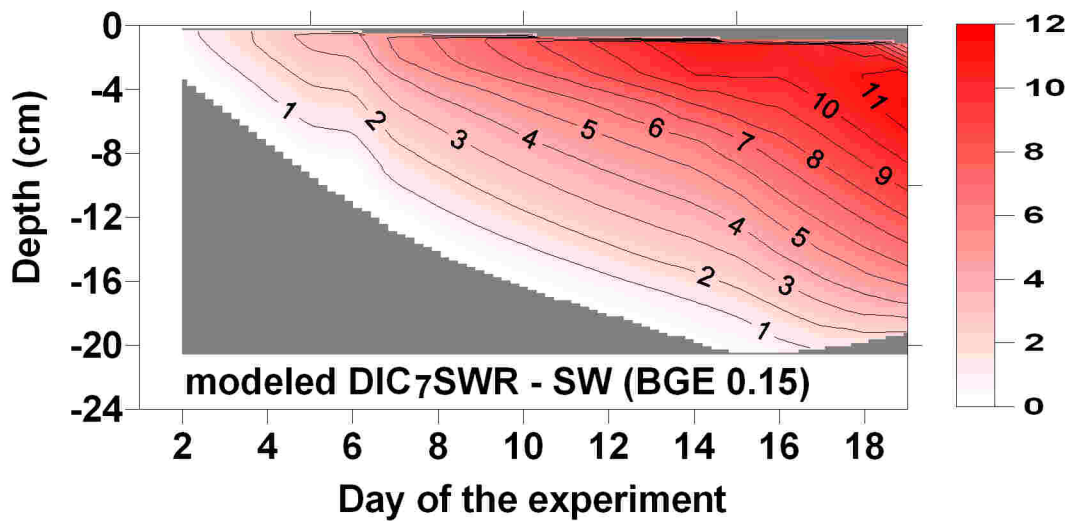
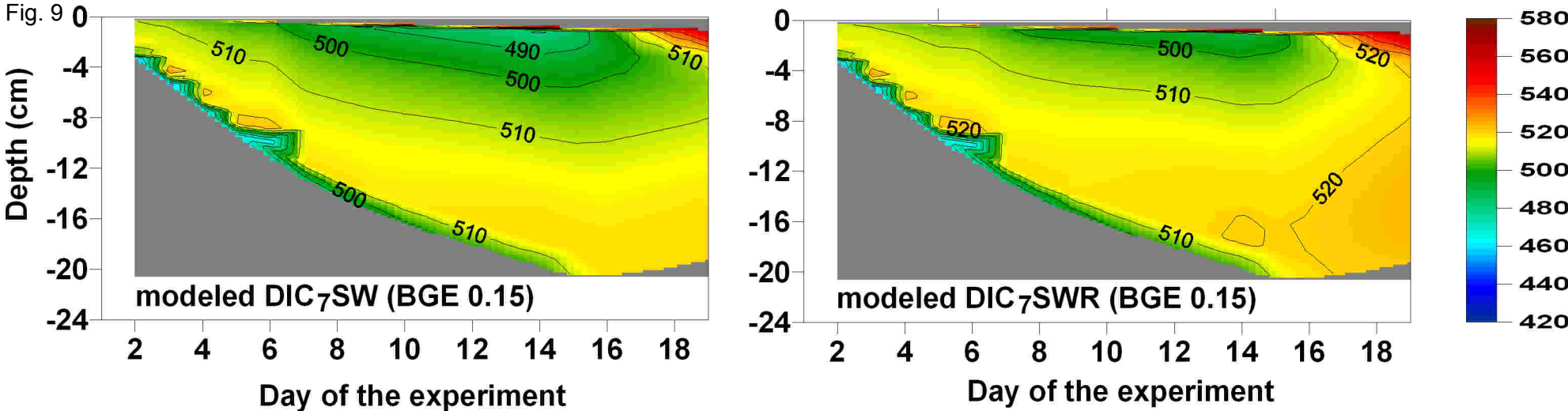


Fig. 10

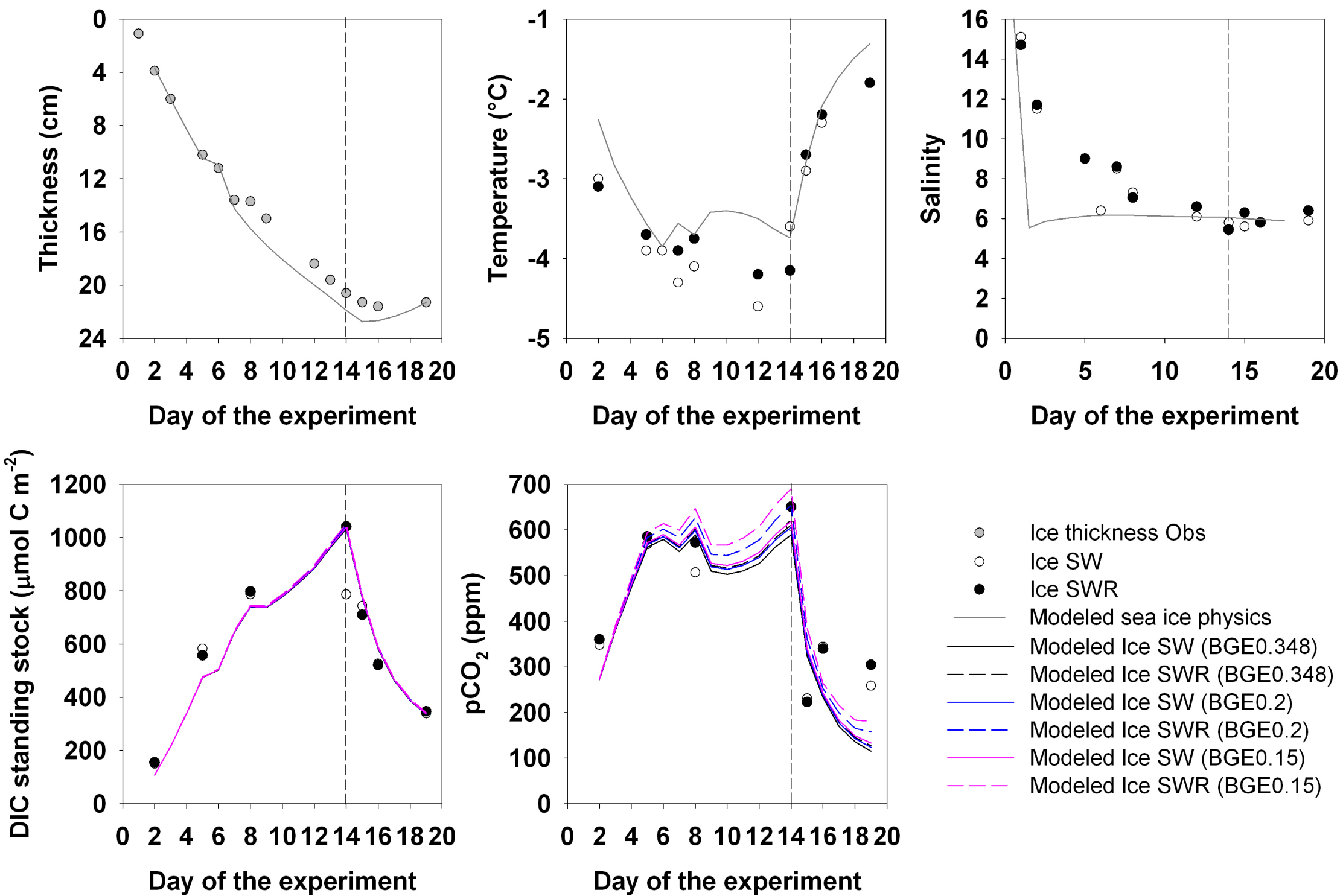


Fig. 110

